Recent development of rare earth lean permanent magnets

Viorel POP

Babeş-Bolyai University, Faculty of Physics,
400084 Cluj-Napoca, Romania

The Scientific research has been conducted by the group of magnetism at UBB

in collaboration with the following teams:

Olivier Isnard
Institut Néel , CNRS, Université Joseph Fourier, Grenoble, France

Ionel Chicinas
Materials Science and Technology Dept., Technical University of Cluj-Napoca, Romania

Jean Marie Le Breton
Groupe de Physique des Matériaux, Université de Rouen, Saint Etienne Du Rouvray, France

Mihaela Văleanu
National Institute of Material Physics, P.O. Box MG-7, R-76900 Magurele, Bucharest, Romania

With the financial supported of
Romanian Ministry of Education and Research, grant PN-II-ID-PCE-2012-4-0470

Outline

- **Introduction**
- **MnBi magnetic phase**
- **MnAl magnetic phase**
- **Nanocomposites magnets=Spring magnets**
- **Conclusions**

Outline

- **Introduction**
- **MnBi magnetic phase**
- **MnAl magnetic phase**
- **Nanocomposites magnets=Spring magnets**
- **Conclusions**

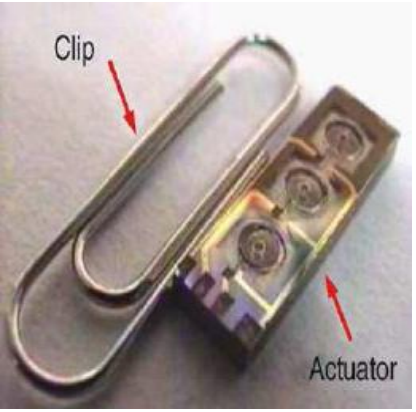

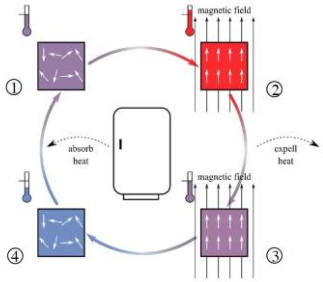

- magnetic materials are ***critical*** components in many devices and for advanced technologies.

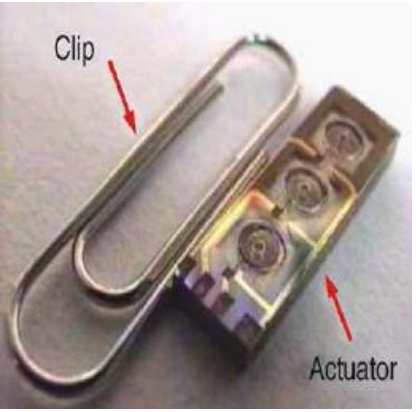

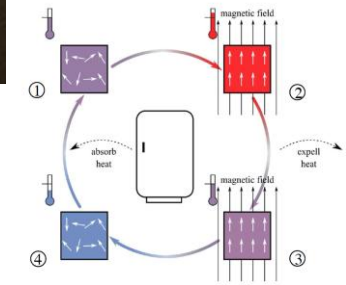

- magnetic materials are ***critical*** components in many devices and for advanced technologies.
- high performance magnet (HPM)/wind generator 1000-1600 kg/MW.
- motors and generators: **2 kg** HPM/hybrid electric vehicle-**20 million** vehicles by 2018.
- Magnetocaloric applications 4 kg HPM/kW cooling power.

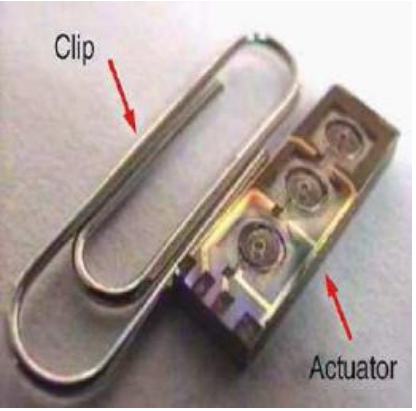

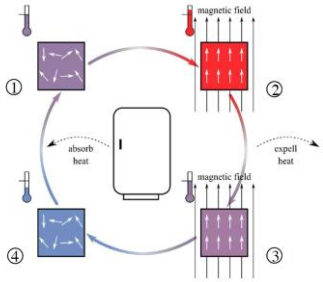

- magnetic materials are ***critical*** components in many devices and for advanced technologies.
- high performance magnet (HPM)/wind generator 1000-1600 kg/MW.
- motors and generators: **2 kg** HPM/hybrid electric vehicle-**20 million** vehicles by 2018.
- Magnetocaloric applications 4 kg HPM/kW cooling power.

HPM= **rare-earth** based magnets

China manages about 96 % of rare-earth resources in 2011

!!!

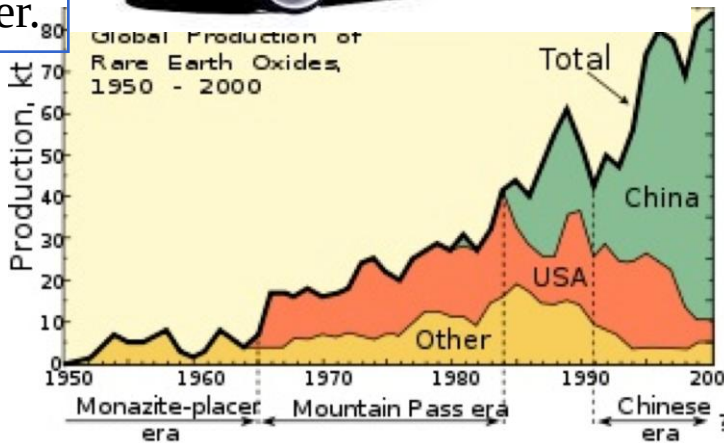

REE price fluctuations

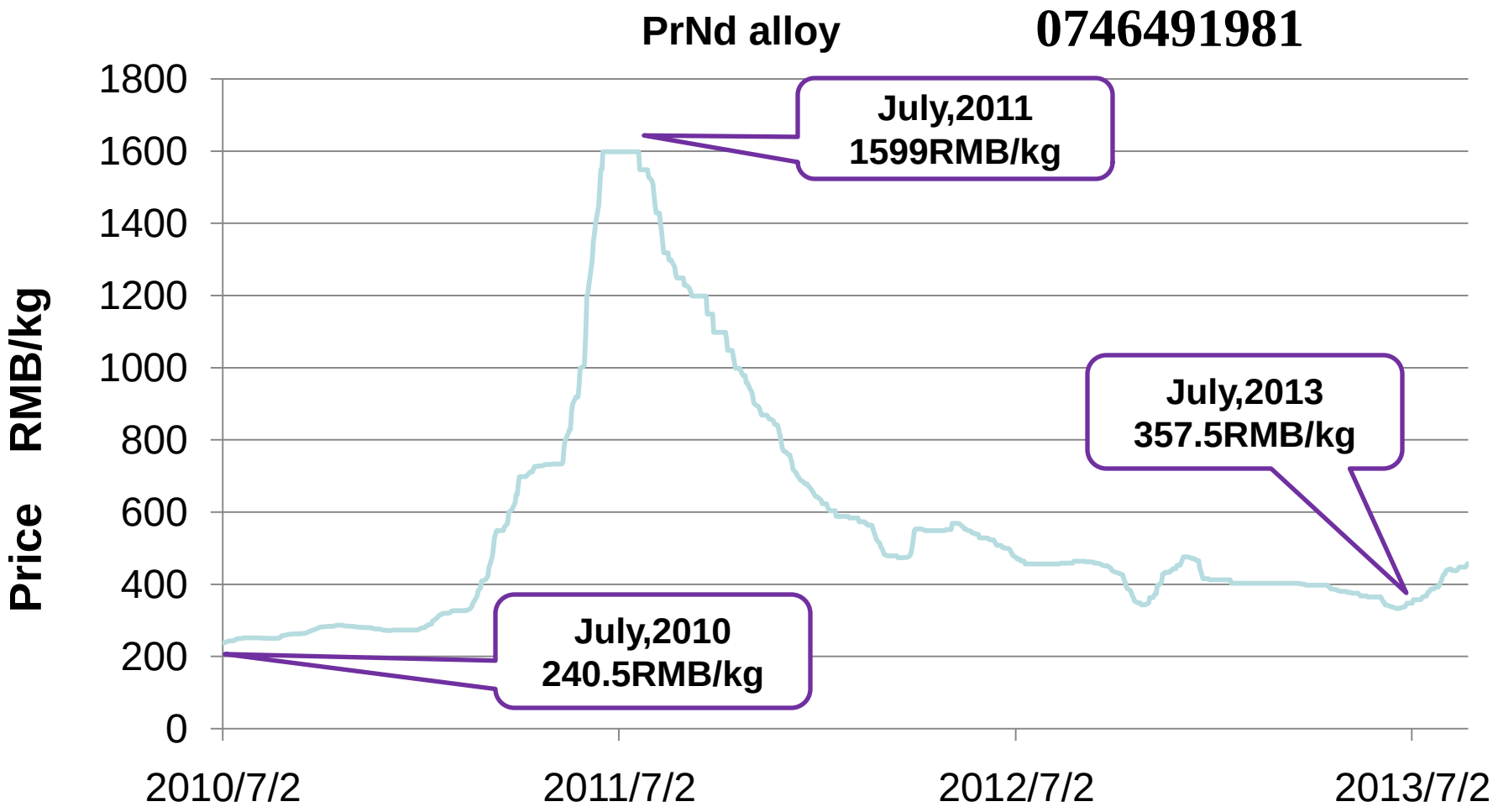

The price of PrNd alloy have increased about 565% form November 2010 to July 2011. In July 2013, it drop to 22.4% compare with top price.

Instability of RE market, ex. Nd: 150 $/kg/2013; 450 $/kg/2011, 15 $/kg/2009

REE price fluctuations

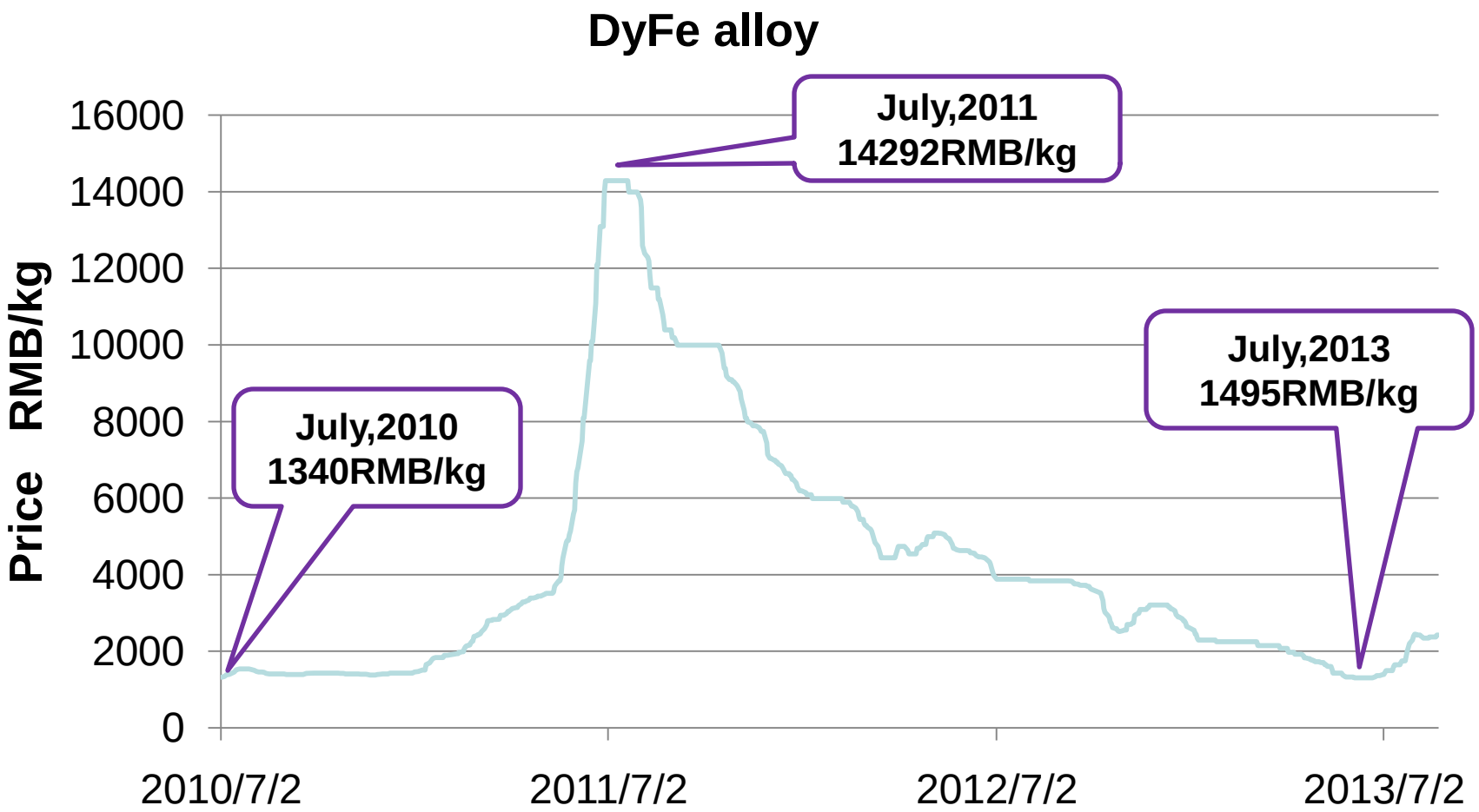

The price of DyFe alloy have increased about 967% form July 2010 to July 2011. In July 2013, it drop to 10.46% compare with top price.

Solutions ?

Solutions ?

Yes, we are obliged to have solutions !

1. The increase of usage efficiency.
2. Recycling.

Solutions ?

Yes, we are obliged to have solutions !

1. The increase of usage efficiency.
2. Recycling.
3. ***New magnetic phases*** without rare-earth with high magnetic properties for applications as permanent magnets and magnetic refrigeration.: Fe-Co si Fe-Ni tetragonal, Fe-Co ternary or quaternary, $Fe_{16}N_2$, MnBi, MnAl, Mn_3Ga, Heusler alloys
4. Soft/hard nanocomposite magnets ➔ ***Spring magnets***

Rare Earth-Free Permanent Magnets ?

✧**RE-free** hard magnetic compounds exist: FePt, CoPt, MnBi, MnAl, Zr_2Co_{11}, ε-Fe_2O_3

✧Even the Alnico-type magnets still have a room for improvement; their theoretical $(BH)_{max}$ is 36-49 MGOe and they have excellent temperature stability; Artificial Alnicos!

Compound	Structure	Saturation magnetization	Curie temperature (°C)	Anisotropy constant K_1 (MJ/m^3)	$(BH)_m$ (MGOe)
Co	hexagonal	17.6 kG	1115	0.53	
FePt	tetragonal	14.3 kG	477	6.6	
CoPt	tetragonal	10.0 kG	567	4.9	
Co_3Pt	hexagonal	13.8 kG	727	2.0	
MnAl	tetragonal	6.2 kG	377	1.7	9.6
MnBi	hexagonal	7.8 kG	357	1.2	16-17
$BaFe_{12}O_{19}$	hexagonal	4.8 kG	450	0.33	3-4
Zr_2Co_{11}	orthorhombic(?)	≈70 emu/g	500	? (H_A = 34 kOe)	14
ε-Fe_2O_3	orthorhombic	≈16 emu/g	?	? (H_c = 23.4 kOe)	
Alnico	Cubic (shape)	12-14			8-11(36)
$SmCo_5$	hexagonal	11.4 kG	681	17.0	25-30
$Nd_2Fe_{14}B$	tetragonal	16.0 kG	312	5.0	30-57

G. Hadjipanayis, Delaware University, Energy and Materials Criticality Workshop, Santorini 2013

Solutions ?

Yes, we are obliged to have solutions !

1. The increase of usage efficiency.
2. Recycling.
3. ***New magnetic phases*** without rare-earth with high magnetic properties for applications as permanent magnets and magnetic refrigeration.: Fe-Co si Fe-Ni tetragonal, Fe-Co ternary or quaternary, $Fe_{16}N_2$, MnBi, MnAl, Mn_3Ga, Heusler alloys
4. Soft/hard nanocomposite magnets ➔ ***Spring magnets***

Our recent research in these directions

1. ***New magnetic phases*** without rare-earth with high magnetic properties

2. **Soft/hard** nanocomposite magnets ➔ ***Spring magnets***

Our recent research in these directions

1. ***New magnetic phases*** without rare-earth with high magnetic properties

   - ✓ ***MnBi***
   - ✓ ***MnAl***
     - $Mn_{50+\delta}Al_{50-\delta}$; $\delta=4$
     - $Mn_{50}Al_{50-\delta}X_{\delta}$; $\delta=4$, X=Ni, Zn, Ti

2. **Soft/hard** nanocomposite magnets ➔ ***Spring magnets***

   - ✓ **hard magnetic phases of $SmCo_5$, $SmCo_3Cu_2$, $R_2Fe_{14}B$**

   - ✓ **soft magnetic phases of α-Fe, Fe-Co (~20 or 10 wt%)**

Our recent research in these directions

1. ***New magnetic phases*** without rare-earth with high magnetic properties

   - ✓ ***MnBi***
   - ✓ ***MnAl***
     - $Mn_{50+\delta}Al_{50-\delta}$; $\delta=4$
     - $Mn_{50}Al_{50-\delta}X_{\delta}$; $\delta=4$, X=Ni, Zn, Ti

2. **Soft/hard** nanocomposite magnets ➔ ***Spring magnets***

   - ✓ **hard magnetic phases of $SmCo_5$, $SmCo_3Cu_2$, $R_2Fe_{14}B$**
     - **$SmCo_5$** **large anisotropy**
     - **$SmCo_3Cu_2$** **large coercivity**
     - **$R_2Fe_{14}B$** **best magnets**
   - ✓ **soft magnetic phases of α-Fe, Fe-Co (~20 or 10 wt%)**

Outline

- Introduction
- **MnBi magnetic phase**
- AlMn magnetic phase
- Nanocomposites magnets=Spring magnets
- Conclusions

MnBi magnetic phase

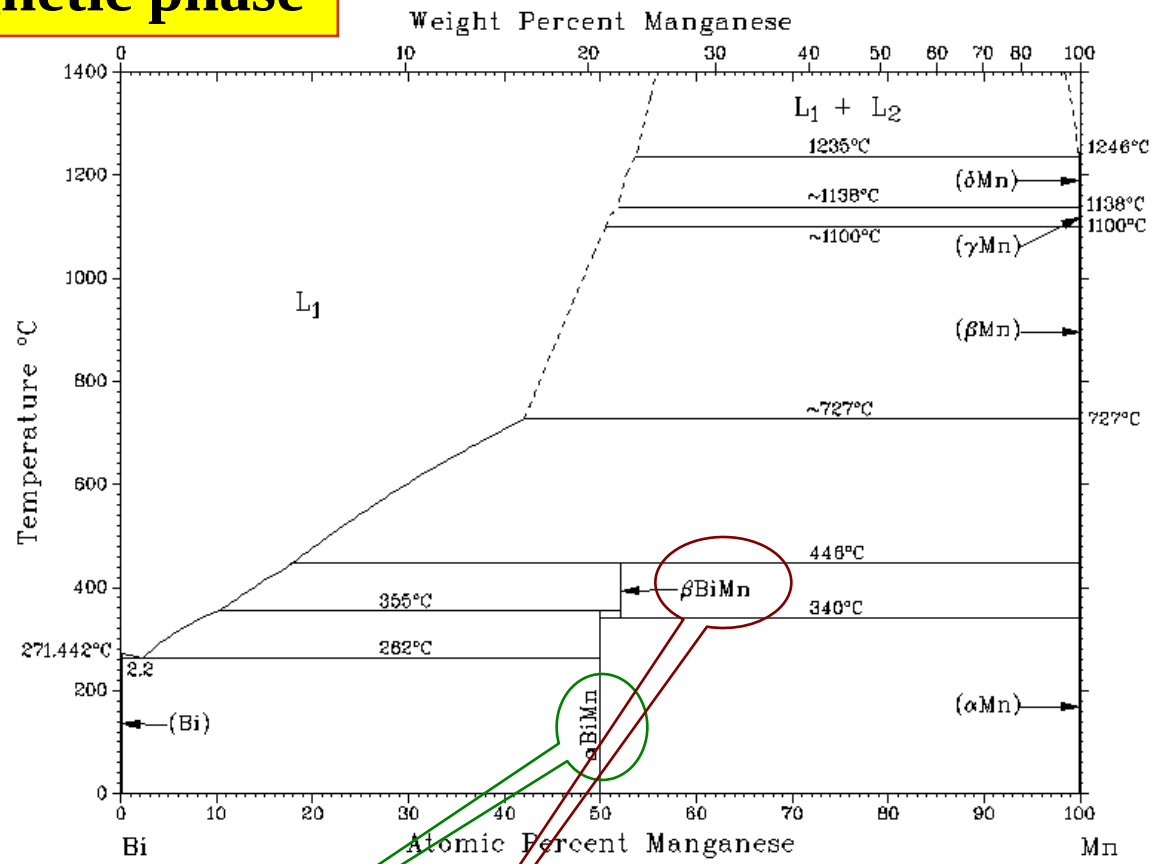

- **Low temperature phase (LTP)-*NiAs type Hexagonal (Ferromagnetic)***
- High temperature phase (HTP) -*Distorted Ni_2In type hexagonal (paramagnetic)*

MnBi magnetic phase

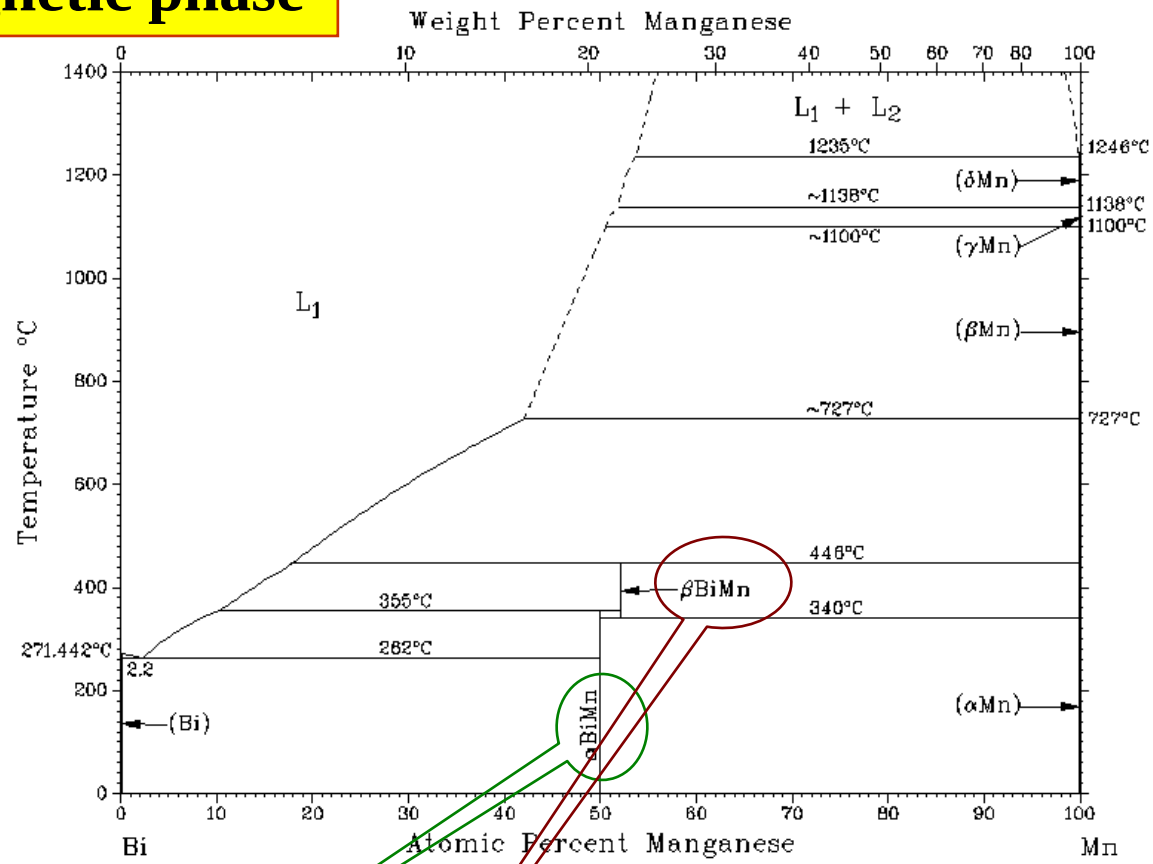

- **Low temperature phase (LTP)-*NiAs type Hexagonal (Ferromagnetic)***
- High temperature phase (HTP) -*Distorted Ni_2In type hexagonal (paramagnetic)*
- Quenched high temperature phase *(QHTP)-Orthorhombic (Ferromagnetic-low M_s)*

Some previous works in MnBi magnetic compound*

Powders: Sintered method & magnetic separation

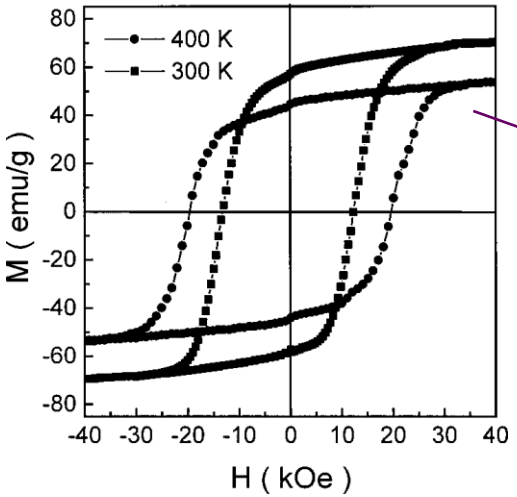

$(BH)_{max}$=7.7 MGOe
(powders)

J B Yang et al. J. Phys.: Condens. Matter 14 (2002) 6509

Nanocrystalline MnBi by melt-spinning technique

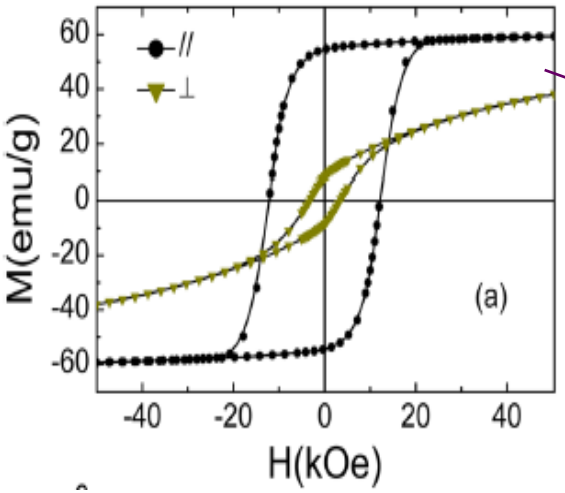

$(BH)_{max}$ = 7.1 MGOe
(powders of melt-spun ribbons)

Yang et al. Appl. Phys. Lett. 99, 082505 (2011)

Hot pressed bulk magnet

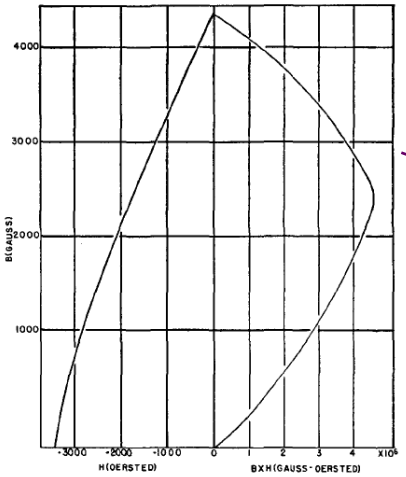

$(BH)_{max}$=4.3 MGOe

Density: 90%

Adams et al. J. Appl. Phys. 23 1207 (1952)

Spark plasma sintered bulk magnet

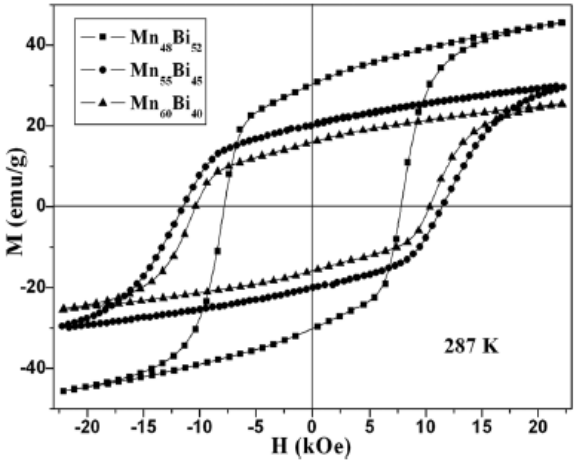

$(BH)_{max}$< 2 MGOe

Density: 93%

Zhang et al. J. Appl. Phys 109, 07A722 (2011)

*G. Hadjipanayis, Delaware University, Energy and Materials Criticality Workshop, Santorini 2013

Magnetic properties of MnBi/$Sm_2Fe_{17}N_x$ nanocomposite powders

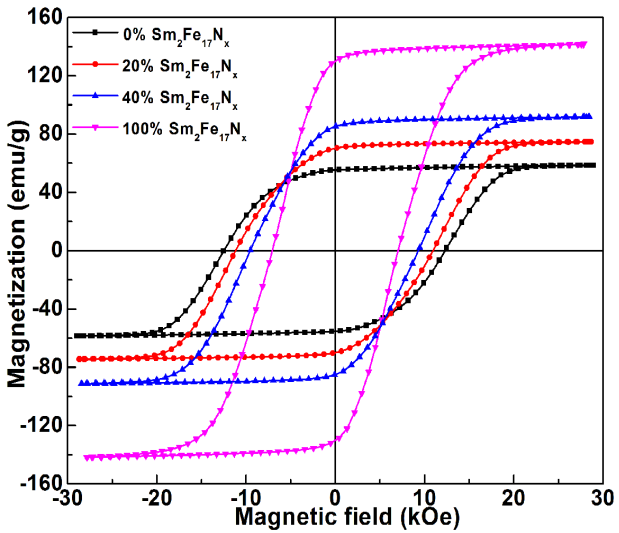

- **MnBi powders: H_c of 12.4 kOe with M_r of 55 emu/g**
- **$Sm_2Fe_{17}N_x$ powders: H_c of 7 kOe with M_r of 130**
- **Hybrid magnet powders exhibit**
  - ***H_c and M_r values intermediate to those of pure MnBi and $Sm_2Fe_{17}N_x$***
  - ***anisotropic magnetic characteristics with M_r/M_s ratio greater than 0.91***

Our main results

MnBi

Synthesis:

- ✓ melting : Mn and Bi of 99,99% purity (1 wt % Mn in excess)
- ✓ annealing : 258-420ºC/ from 2 hours to 4 days
- ✓ mechanical milling: of bulk MnBi phase for 2 hours

X-rays powder diffraction:

- ✓ K_{α} radiation of copper in the angular range 2θ = 20 - 100° and
- ✓ $K_{\alpha 1}$ radiation of cobalt in angular range 2θ= 20 - 80º

Magnetic measurements:

- ✓ extraction method in a continuous magnetic field of up to ± 10 T

MnBi: influence of ***annealing***

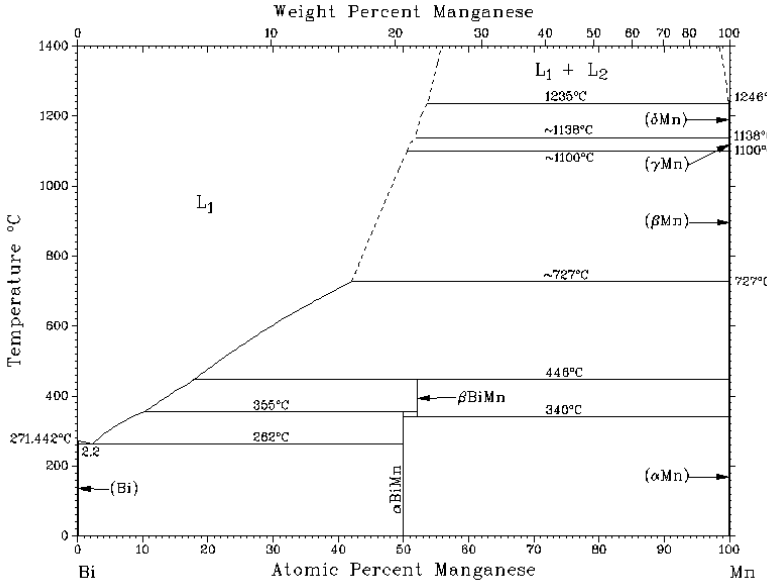

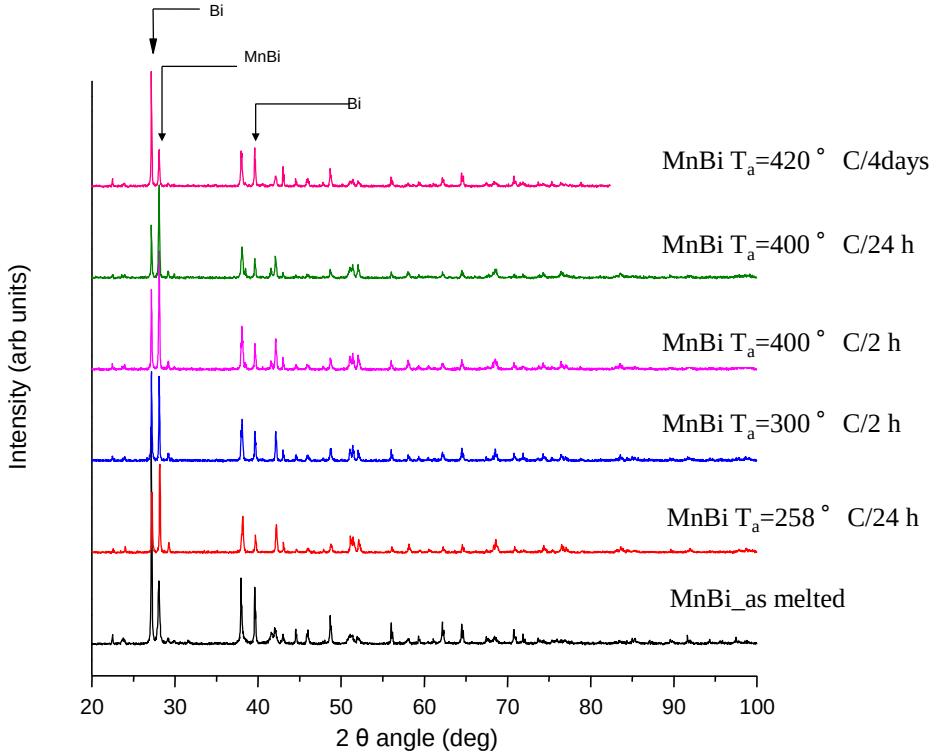

MnBi: influence of ***annealing***; XRD Cu K_α radiation

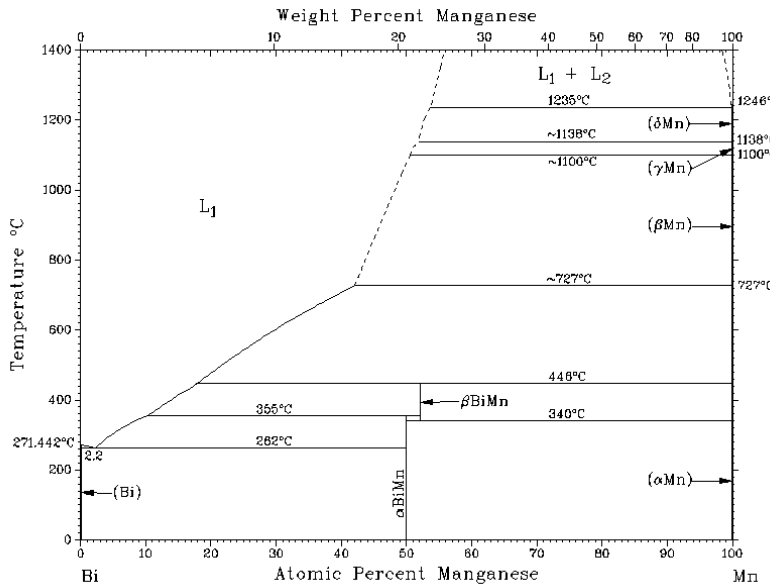

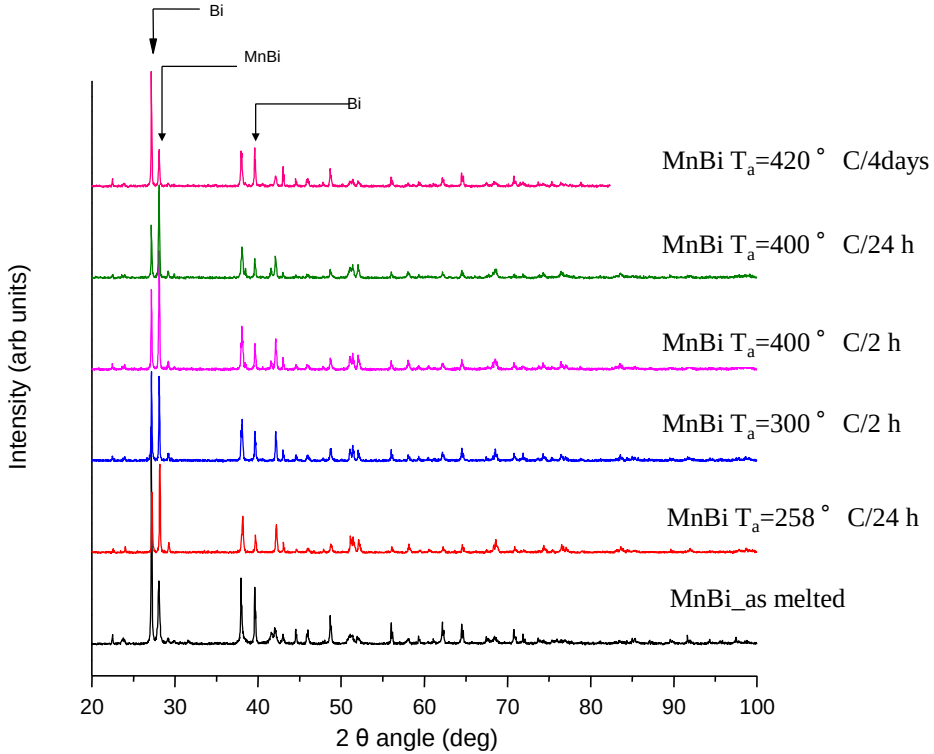

MnBi: influence of ***annealing***; XRD Cu K_α radiation

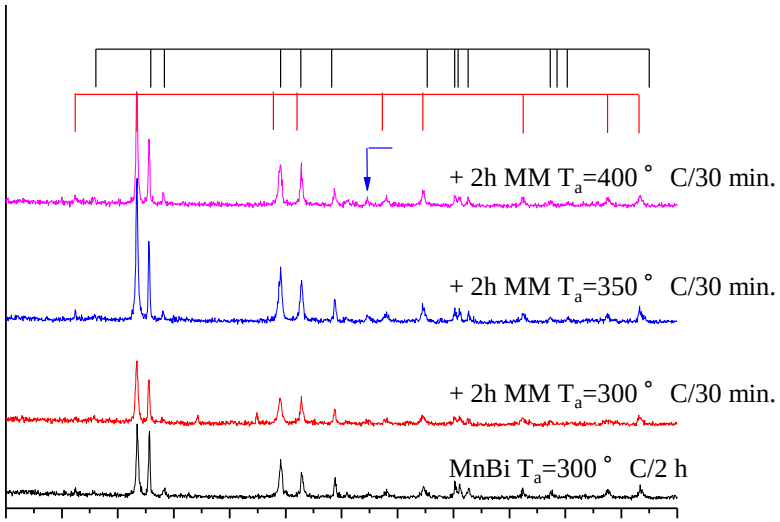

MnBi: influence of ***milling***; XRD Co K_α radiation

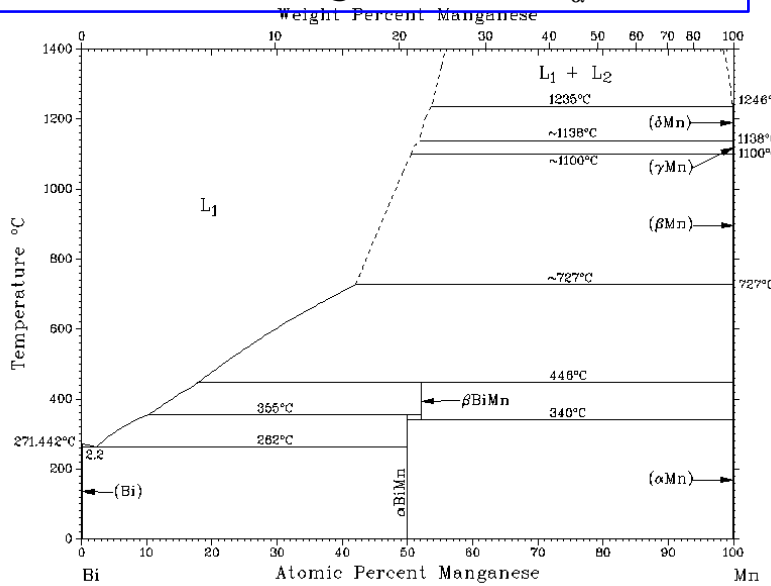

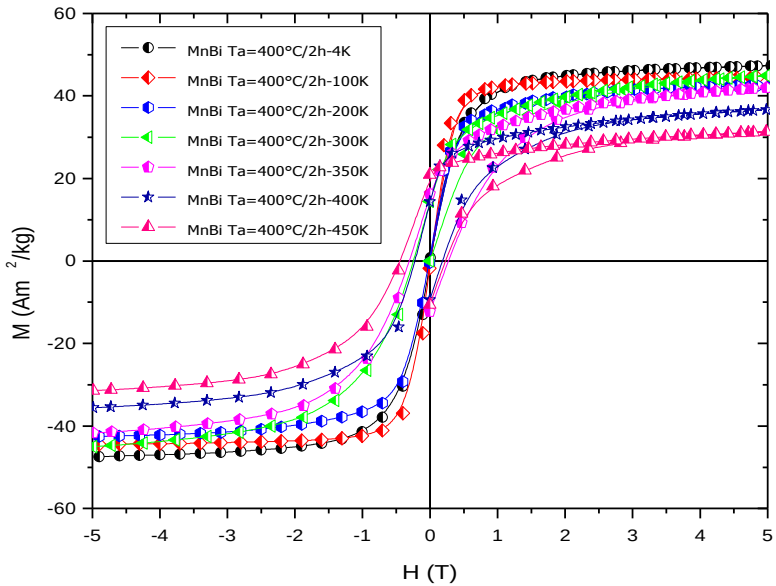

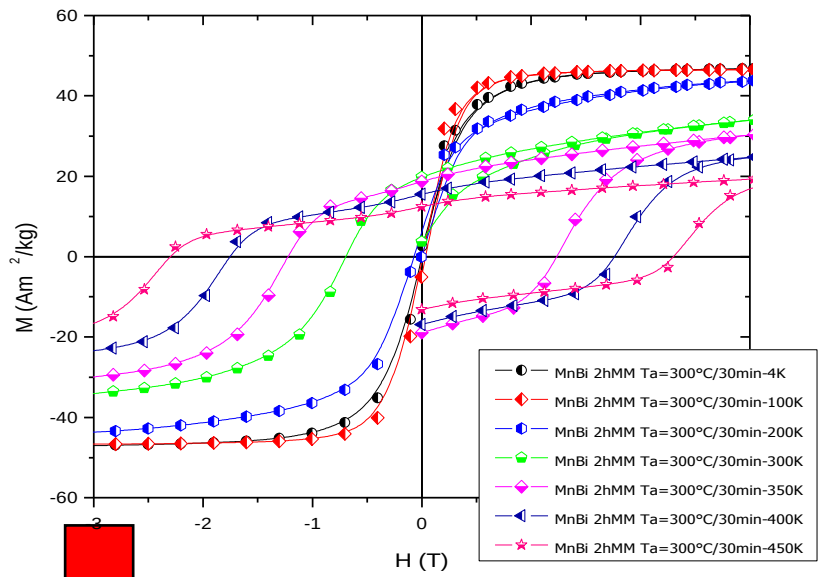

M(H) for different T,
MnBi melted samples, annealed at 400ºC for 2 h

Hysteresis loops for different T,
MnBi 2h MM+TT 300 ºC/30 min

Important coercivity at high temperature, competition with REPM

Outline

- Introduction
- MnBi magnetic phase
- **MnAl magnetic phase**
- Nanocomposites magnets=Spring magnets
- Conclusions

Mn-Al magnetic phase

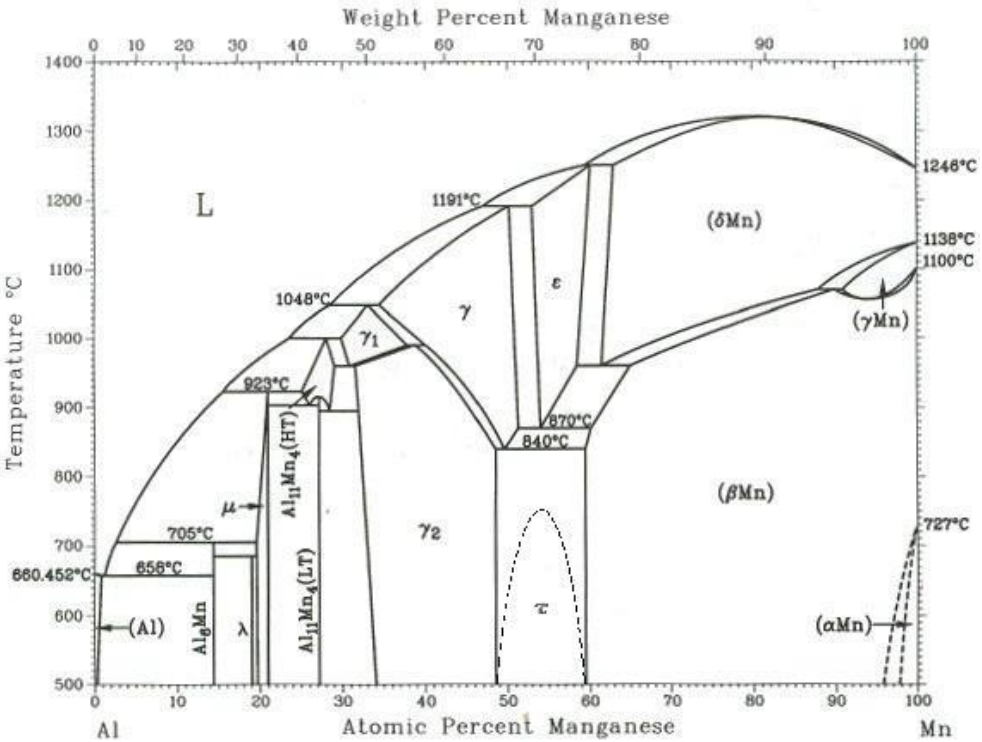

Mn-Al magnetic phase

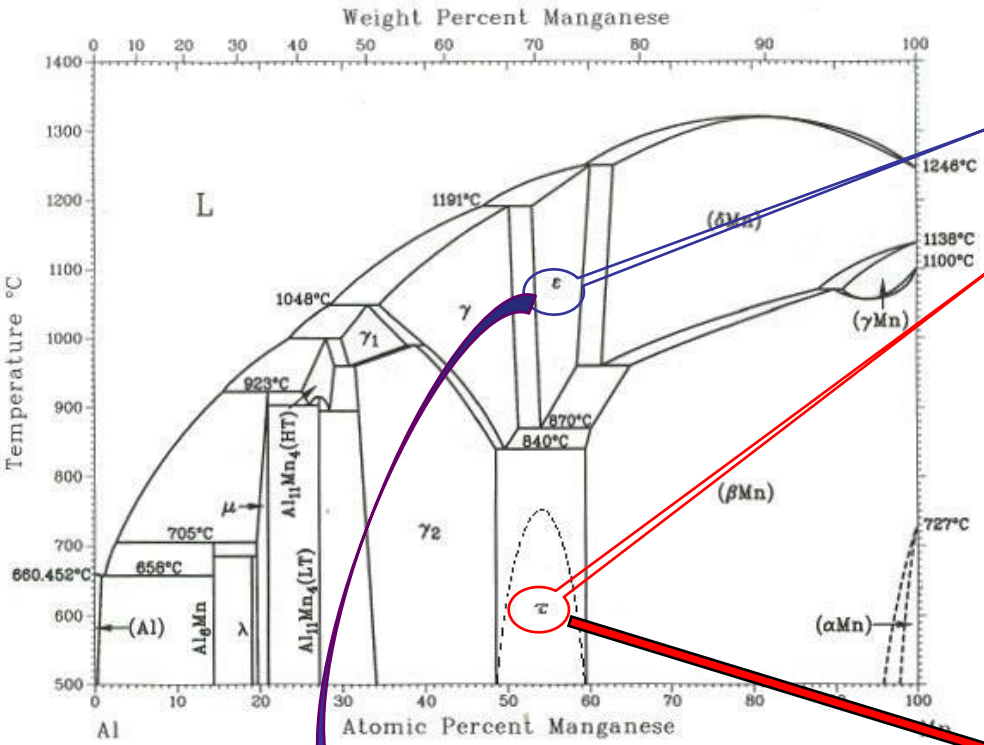

ε phase –

antiferromagnetic hexagonal struct**ure**

τ phase –

$L1_0$- ferromagnetic tetragonal structure

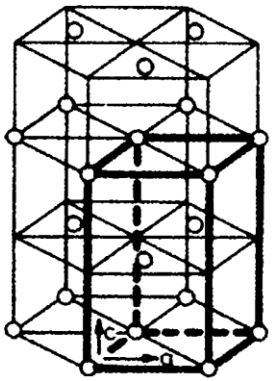

A3 (ε)

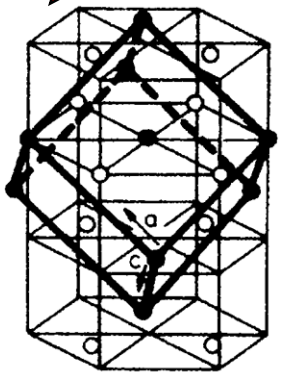

$L1_0(\tau)$

Mn-Al magnetic phase

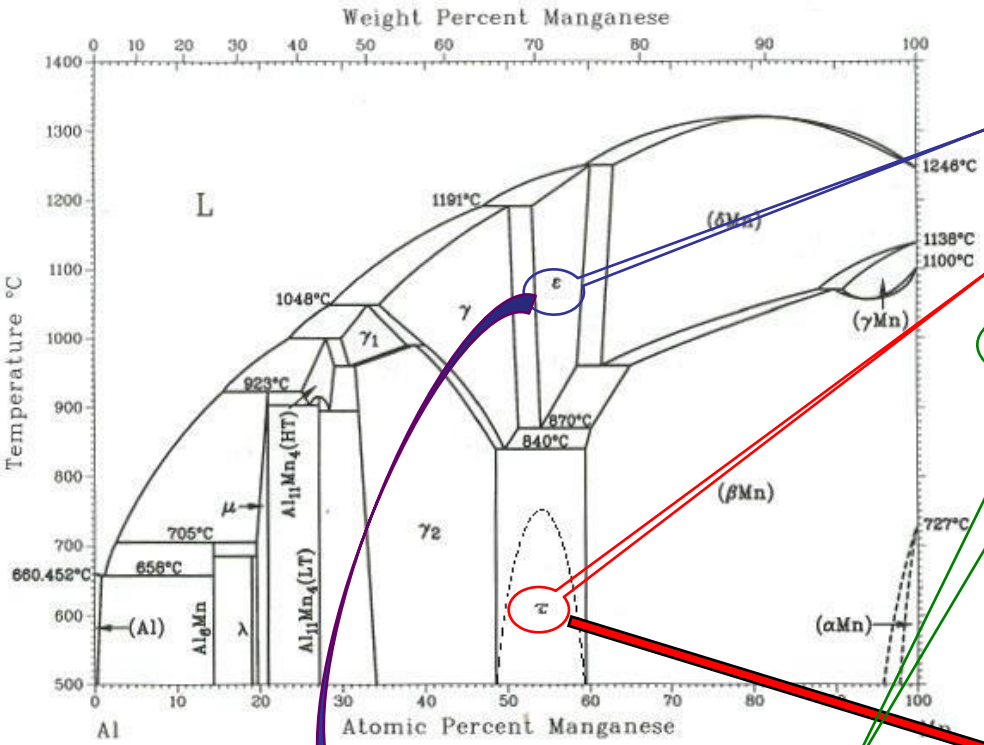

ε phase –

antiferromagnetic hexagonal structure

τ phase –

$L1_0$- ferromagnetic tetragonal structure

ε' phase –

Intermediate ferromagnetic ***ordered*** orthorhombic phase

$Mn_{54}Al_{46}$- the best results

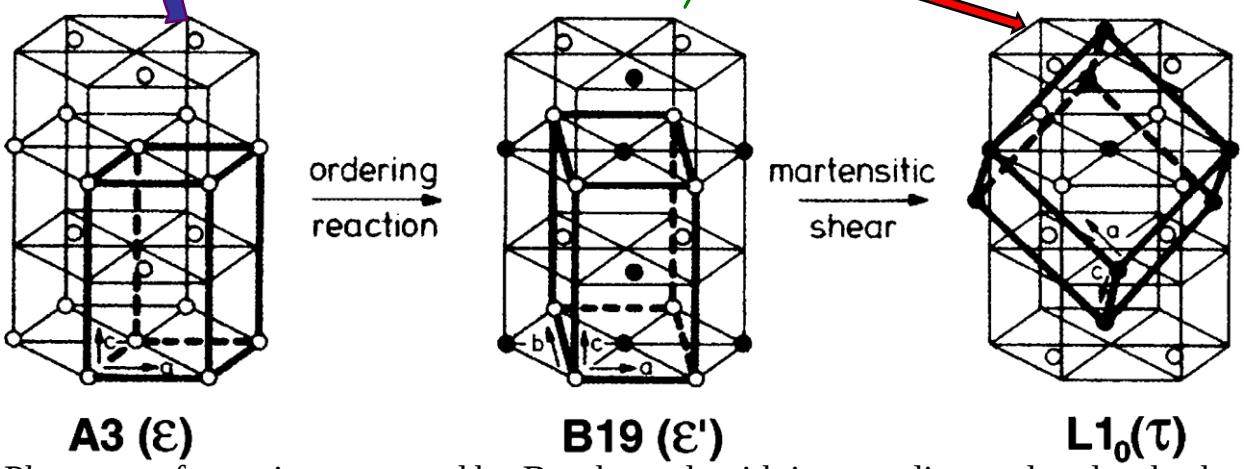

- Phase transformation proposed by Broek et. al. with intermediate ordered orthorhombic phase (B19) denoted by ε'.
- Acta Metall.,27(1979) 1497

Phase formation, microstructure, magnetic properties of the Mn–Al–C; bulk or MM*

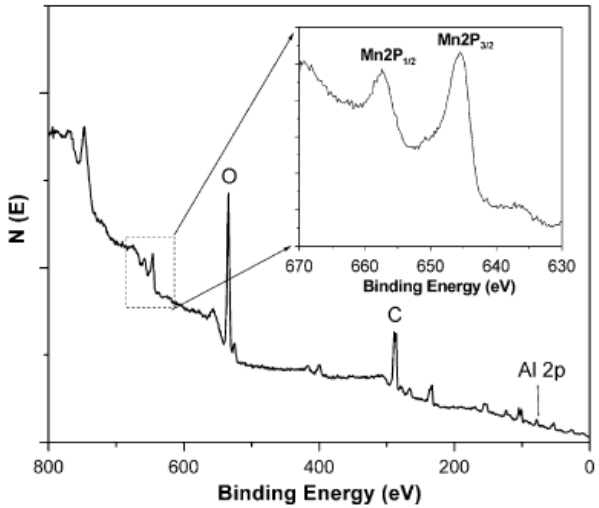

Fig. 4. XPS spectrum of an annealed $Mn_{54}Al_{46}$. The inset is the corresponding spectrum of Mn2p.

τ-phase nucleates almost exclusively at the ***ε-phase grain boundaries***

*Q. Zeng, I. Baker, J.B. Cui, Z.C. Yan, JMMM, 308 (2007) 214–226

Phase formation, microstructure, magnetic properties of the Mn–Al–C; bulk or MM*

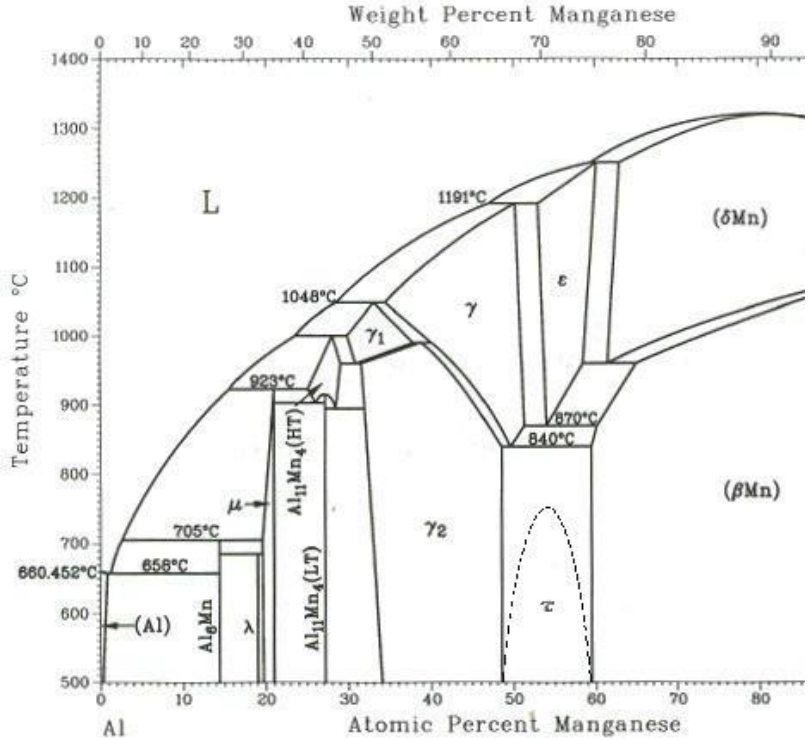

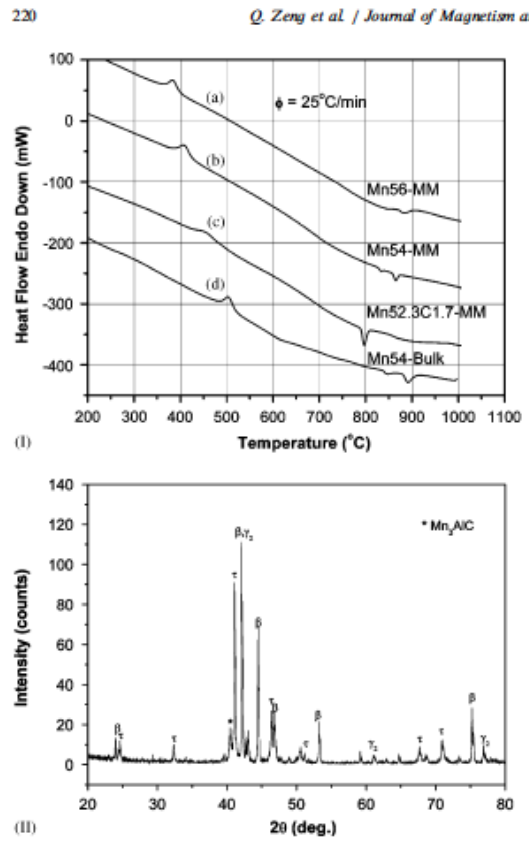

Fig. 7. (I) DTA curves for (a) MM $Mn_{56}Al_{44}$, (b) MM $Mn_{54}Al_{46}$, (c) $Mn_{52.3}Al_{46}C_{1.7}$, and (d) bulk $Mn_{54}Al_{46}$. The heating rate was 25 °C/min. (II) XRD pattern for MM $Mn_{52.3}Al_{46}C_{1.7}$ heated to 760 °C at the heating rate of 25 °C/min and quenched.

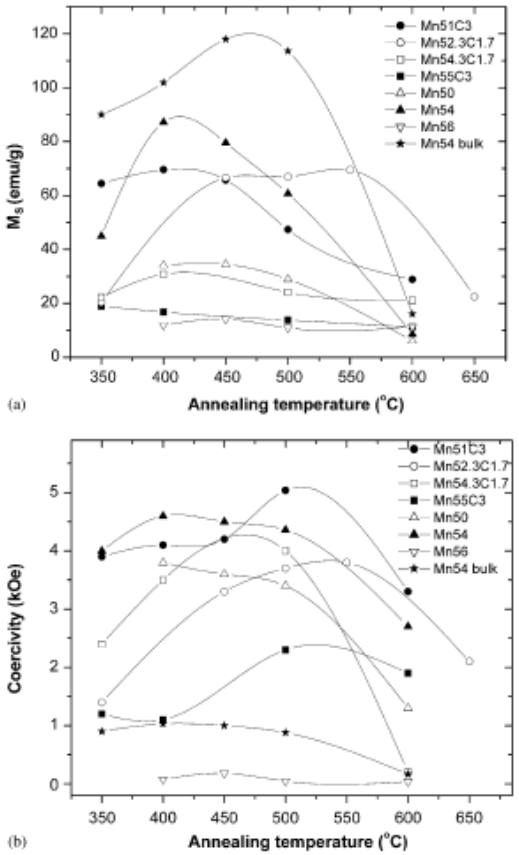

Fig. 8. Dependence of M_S and H_C on the annealing temperatures for MM and bulk samples with various compositions as indicated. The annealing time was 30 min.

- DSC: the transformation **ε(ε')→ τ phase**,
- **τ** –phase stabilized by C doping,
- C doping *cannot prevent* the formation of the equilibrium phases from the metastable ε -phase during annealing.

*Q. Zeng, I. Baker, J.B. Cui, Z.C. Yan, JMMM, 308 (2007) 214–226

Phase formation, microstructure, magnetic properties of the Mn–Al–C; bulk or MM*

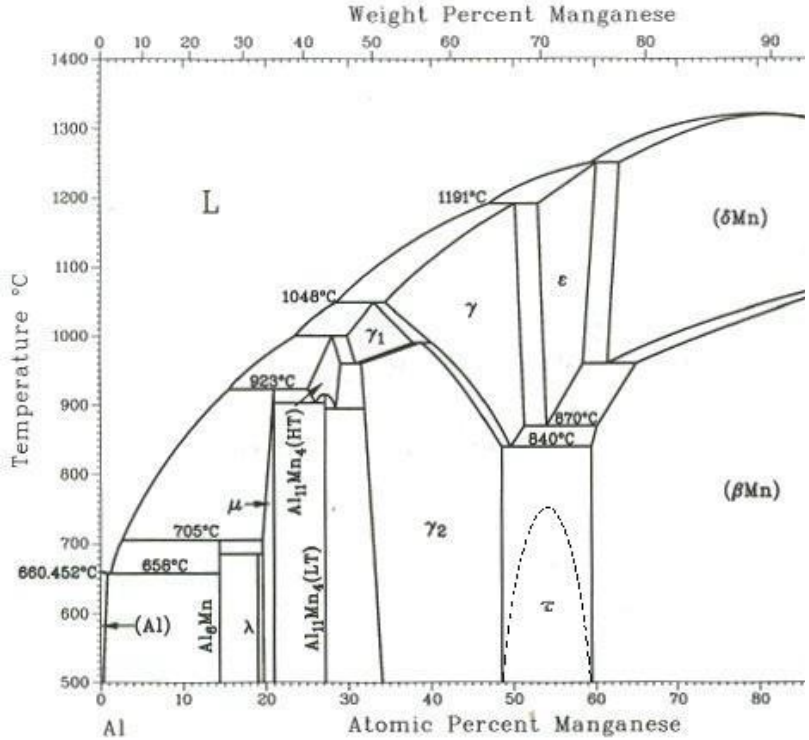

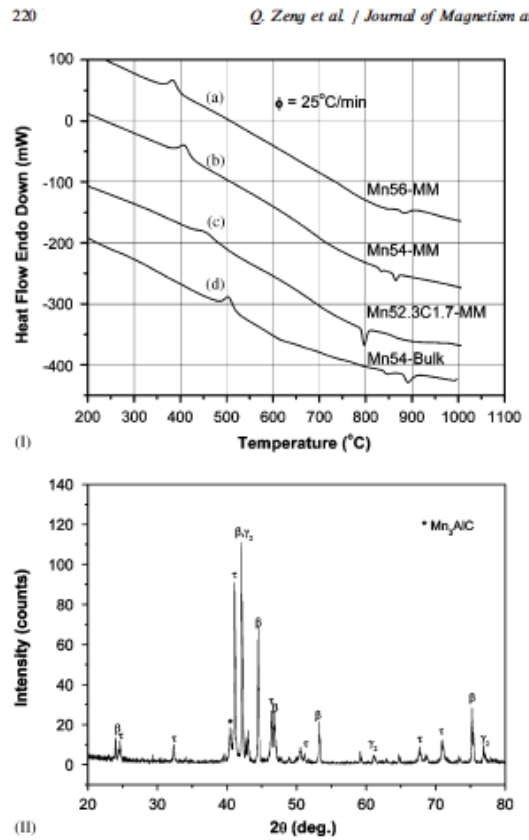

Fig. 7. (I) DTA curves for (a) MM $Mn_{56}Al_{44}$, (b) MM $Mn_{54}Al_{46}$, (c) $Mn_{52.3}Al_{46}C_{1.7}$, and (d) bulk $Mn_{54}Al_{46}$. The heating rate was 25 °C/min. (II) XRD pattern for MM $Mn_{52.3}Al_{46}C_{1.7}$ heated to 760 °C at the heating rate of 25 °C/min and quenched.

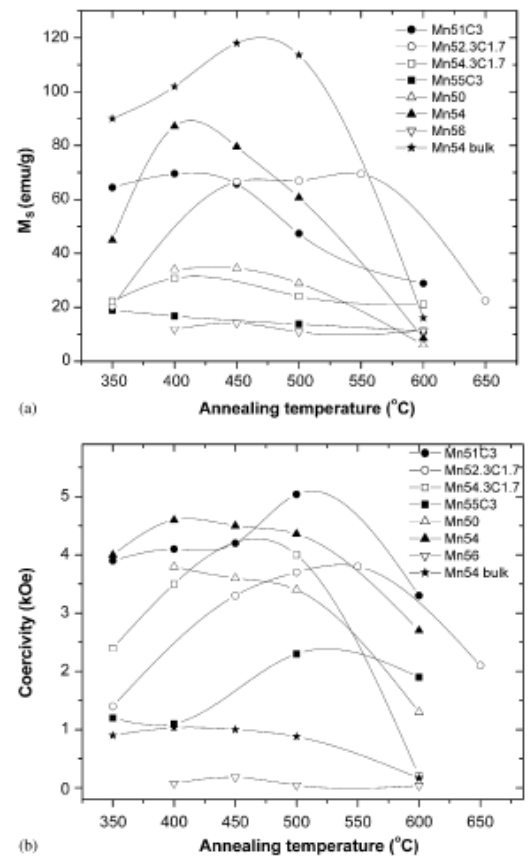

Fig. 8. Dependence of M_S and H_C on the annealing temperatures for MM and bulk samples with various compositions as indicated. The annealing time was 30 min.

- DSC: the transformation **ε(ε')→ τ phase**,
- **τ** –phase stabilized by C doping,
- C doping *cannot prevent* the formation of the equilibrium phases from the metastable ε -phase during annealing.

The optimal magnetic properties for the MM samples, H_c=4.8 kOe, M_r=45 emu/g and M_s= 89 emu/g, were obtained for $Mn_{54}Al_{46}$ annealed at 400 ° C for 10 min

*Q. Zeng, I. Baker, J.B. Cui, Z.C. Yan, JMMM, 308 (2007) 214–226

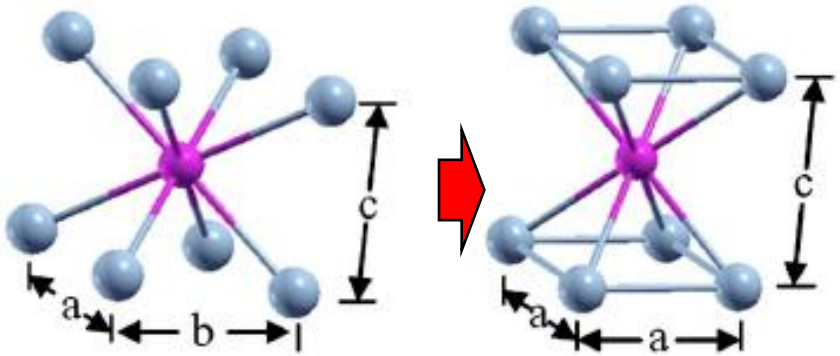

ε'-phase τ-phase.

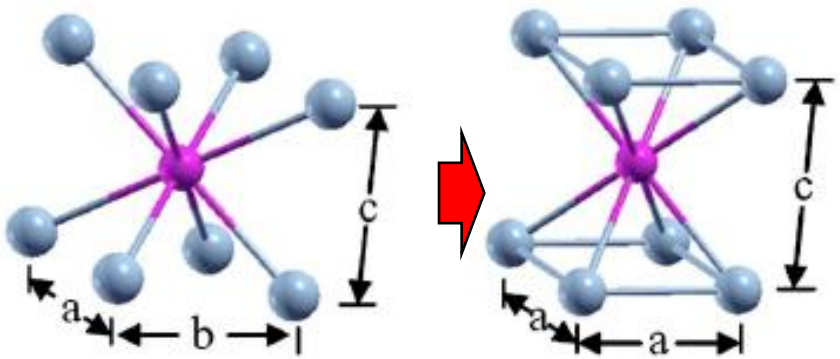

ε'-phase τ-phase.

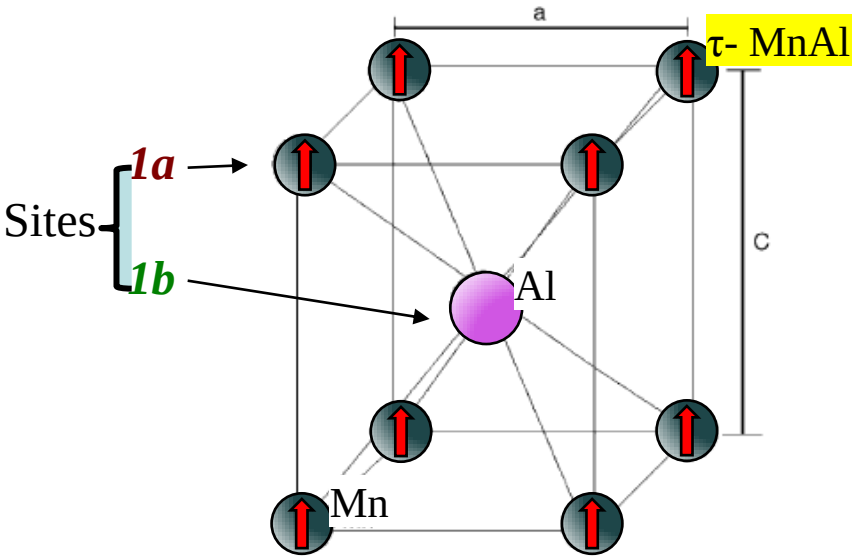

K. Anand et al. / Journal of Alloys and Compounds 601 (2014) 234–237

(a)the total density of states

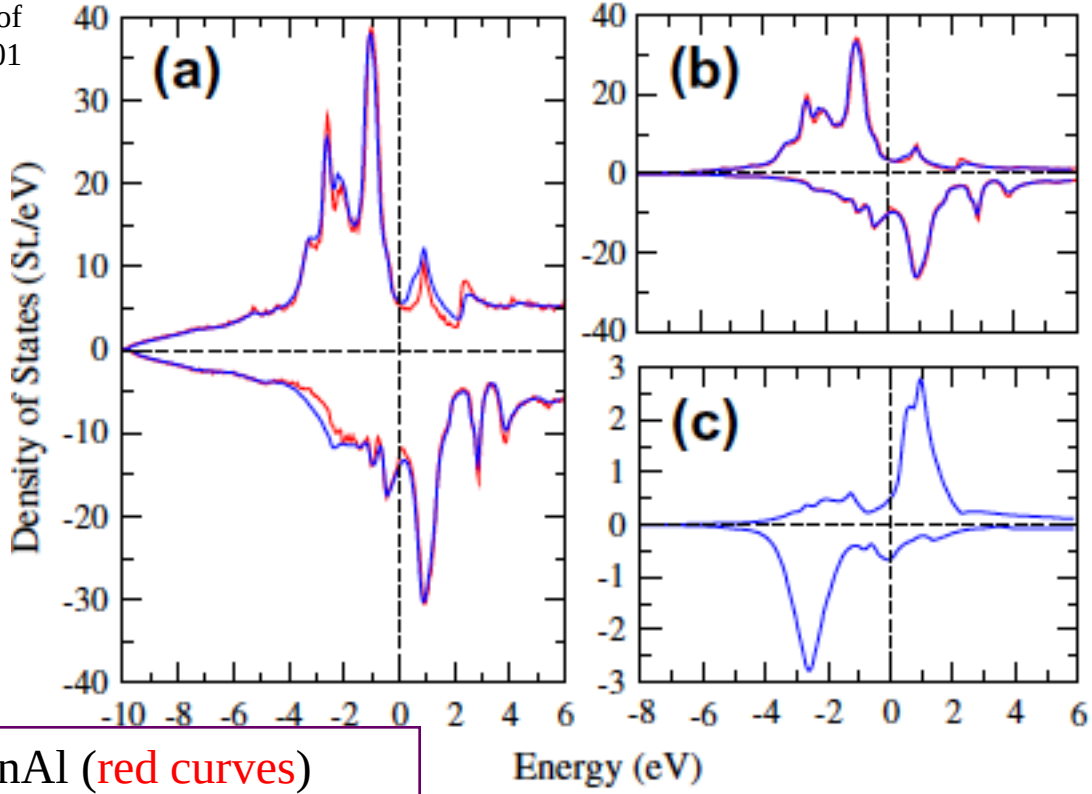

(b) the 3d partial density of states of **Mn at the *1a* site**

(c) the 3d partial density of states of **Mn at the *1b* site** of the P4/mmm unit cell

stoichiometric MnAl (red curves)
$Mn_{50+\delta}Al_{50-\delta}$; δ=4 (blue curves) .

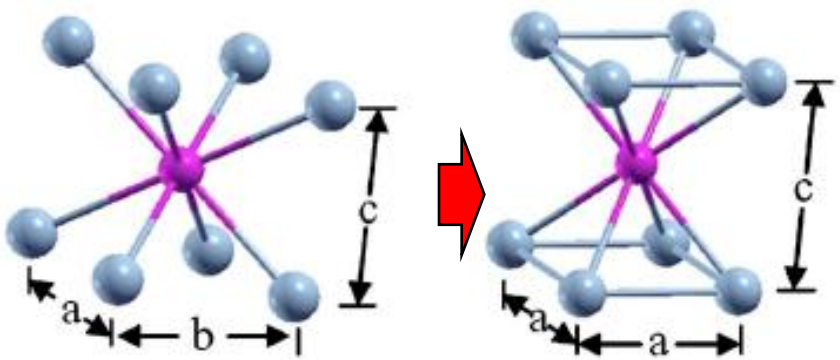

ε'-phase τ-phase.

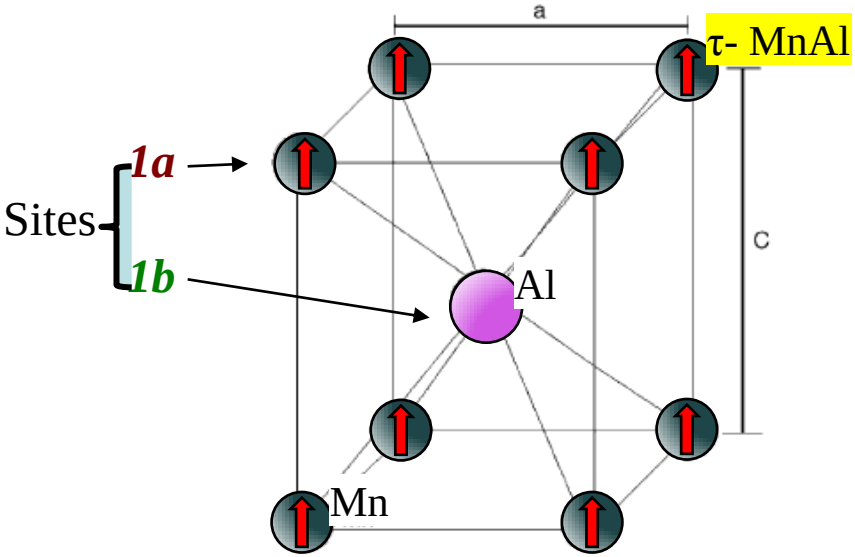

Our results

$Mn_{50}Al_{46}Ni_4$ and $Mn_{54}Al_{46}$

- Ingots were prepared by arc or induction melting
- Different heat treatment to stabilize the desired magnetic phase

Measurements

- Differential thermal analysis (DTA)
- XRD on Brüker D8 Advance diffractometer
- Thermomagnetic measurements up to 800 K

DTA_$Mn_{50}Al_{46}Ni_4$ and $Mn_{54}Al_{46}$

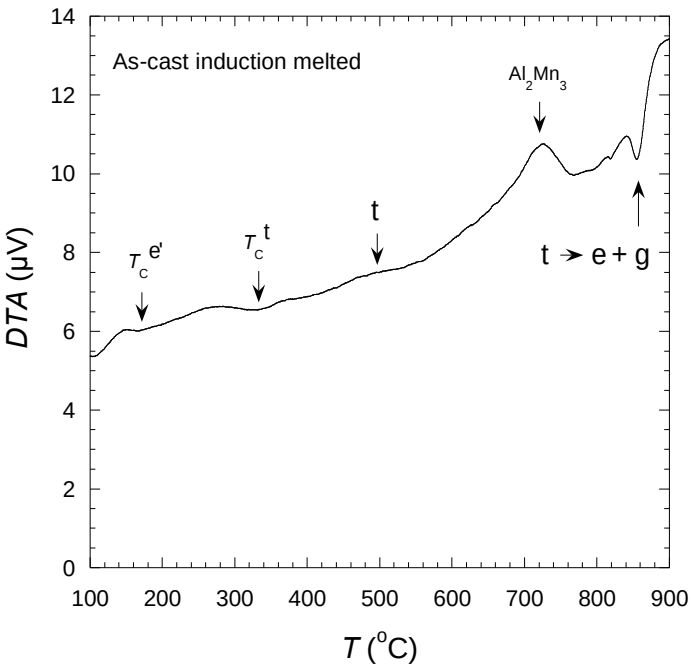

Fig. 1. DTA curve for the as-cast $Mn_{50}Al_{46}Ni_4$ alloy.

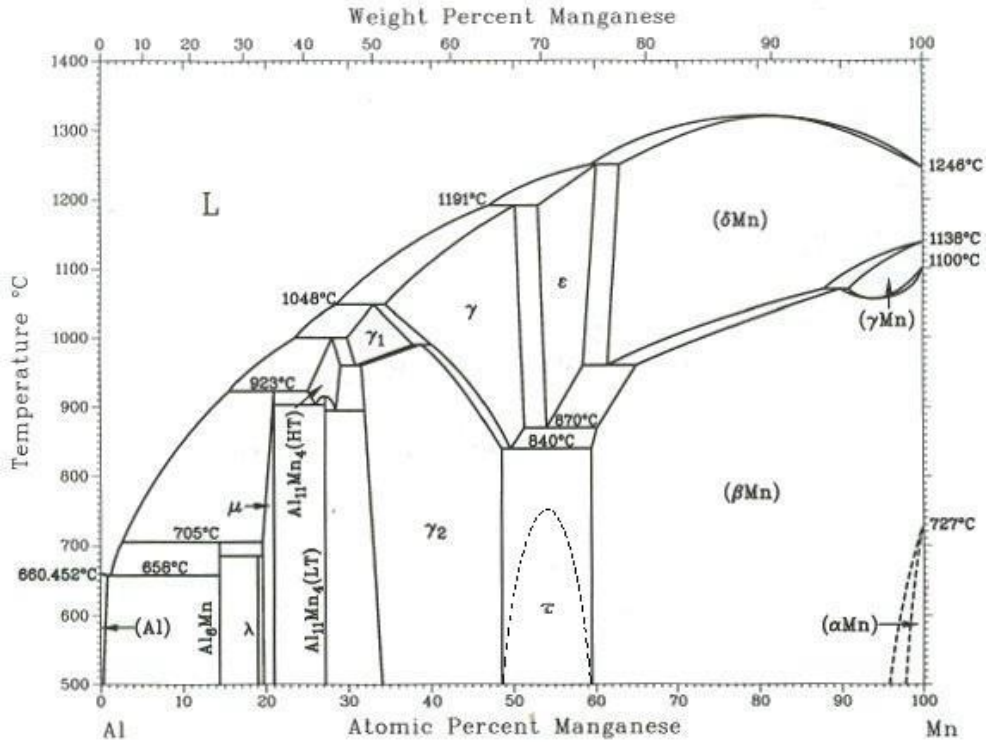

XRD_$Mn_{50}Al_{46}Ni_4$ and $Mn_{54}Al_{46}$

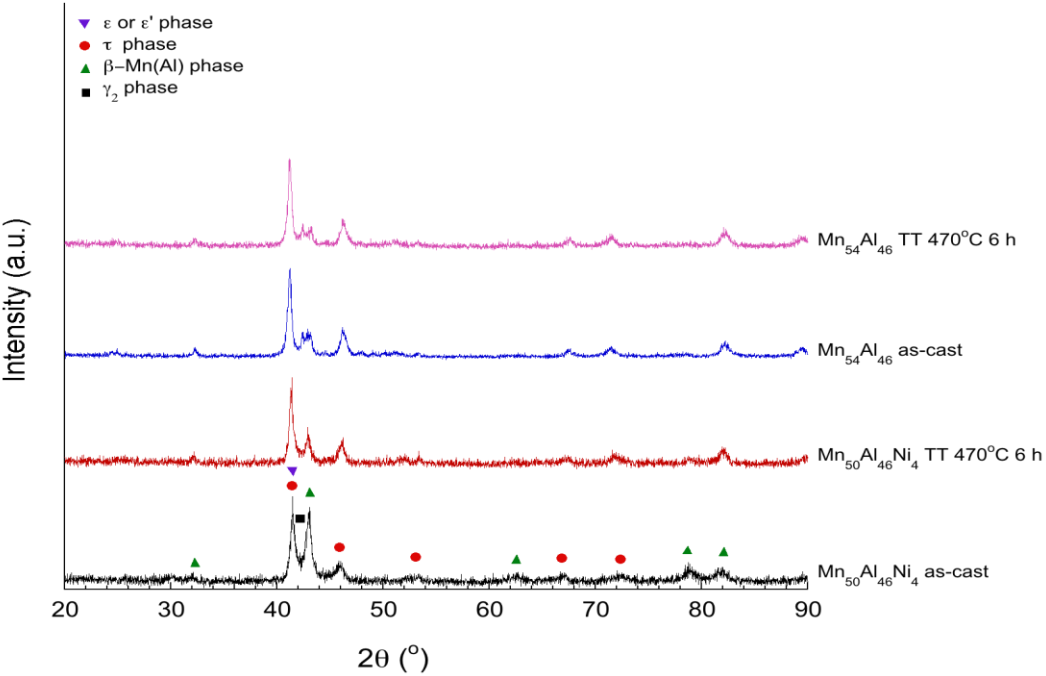

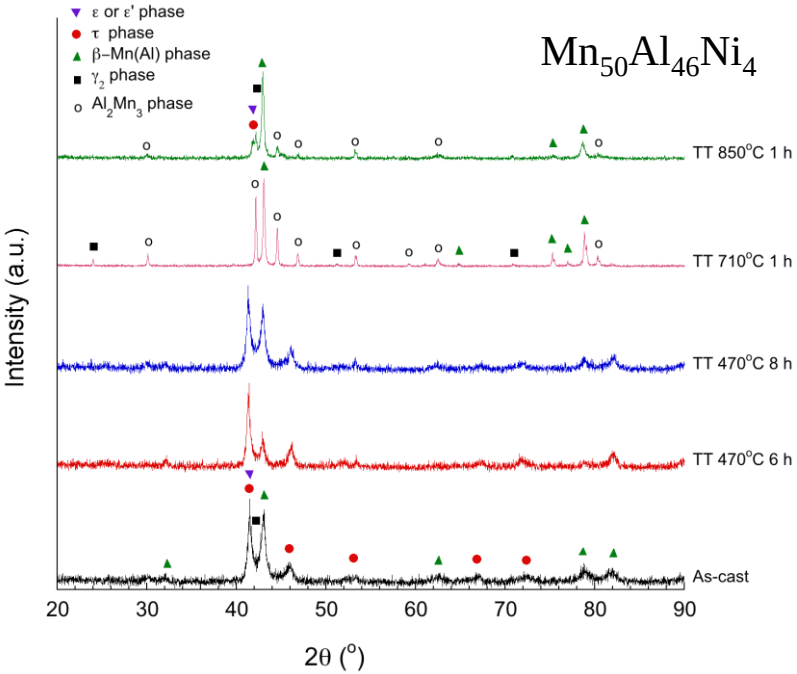

Thermomagnetic studies

$Mn_{50}Al_{46}Ni_4$ and $Mn_{54}Al_{46}$

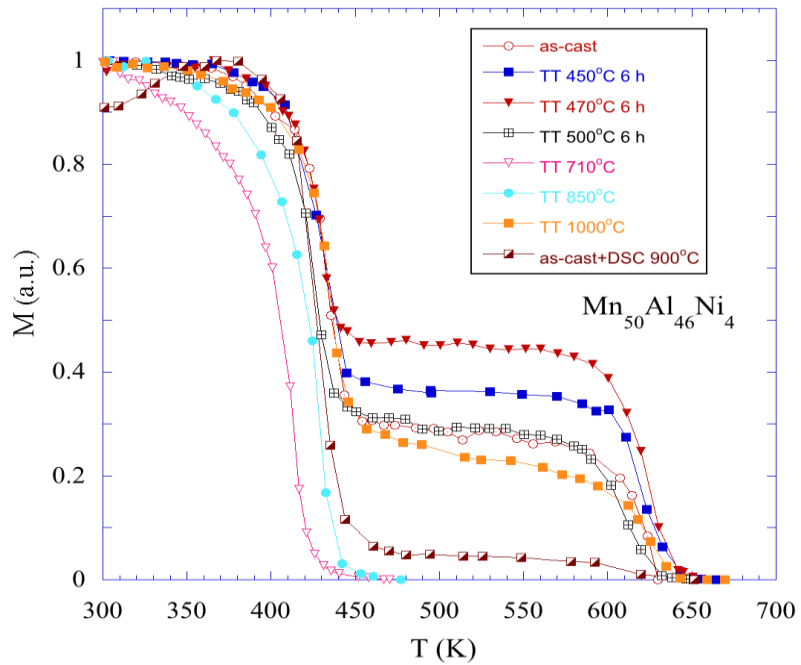

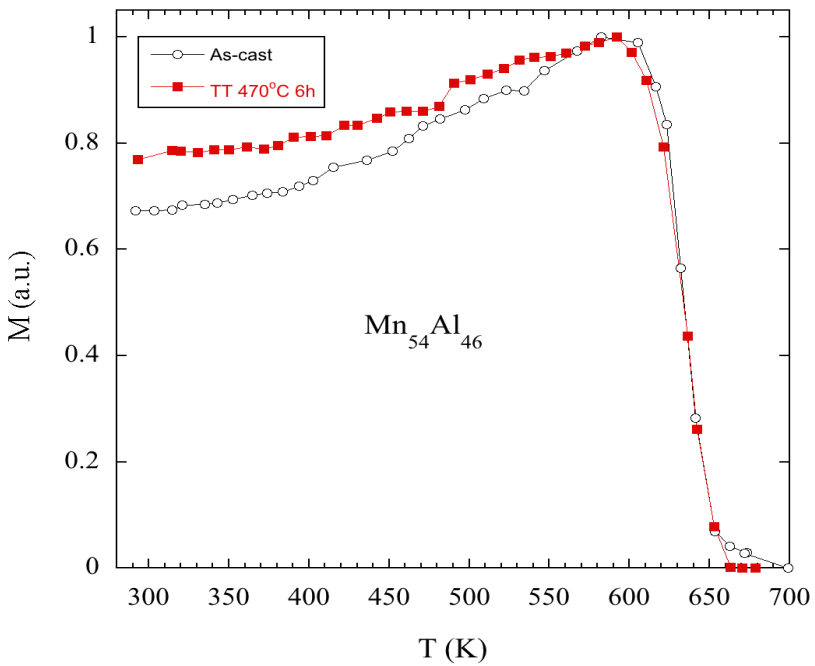

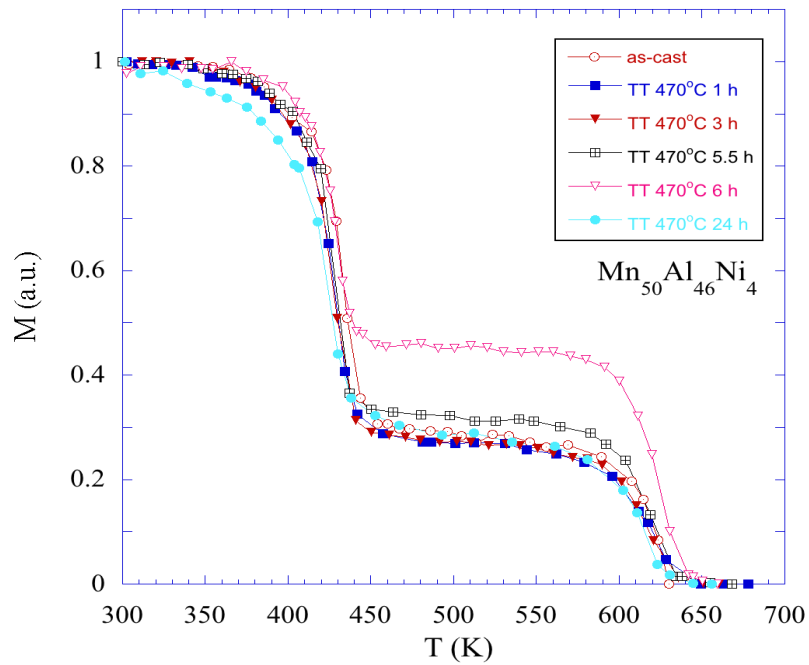

Paramagnetic behavior

$Mn_{50}Al_{46}Ni_4$ and $Mn_{54}Al_{46}$

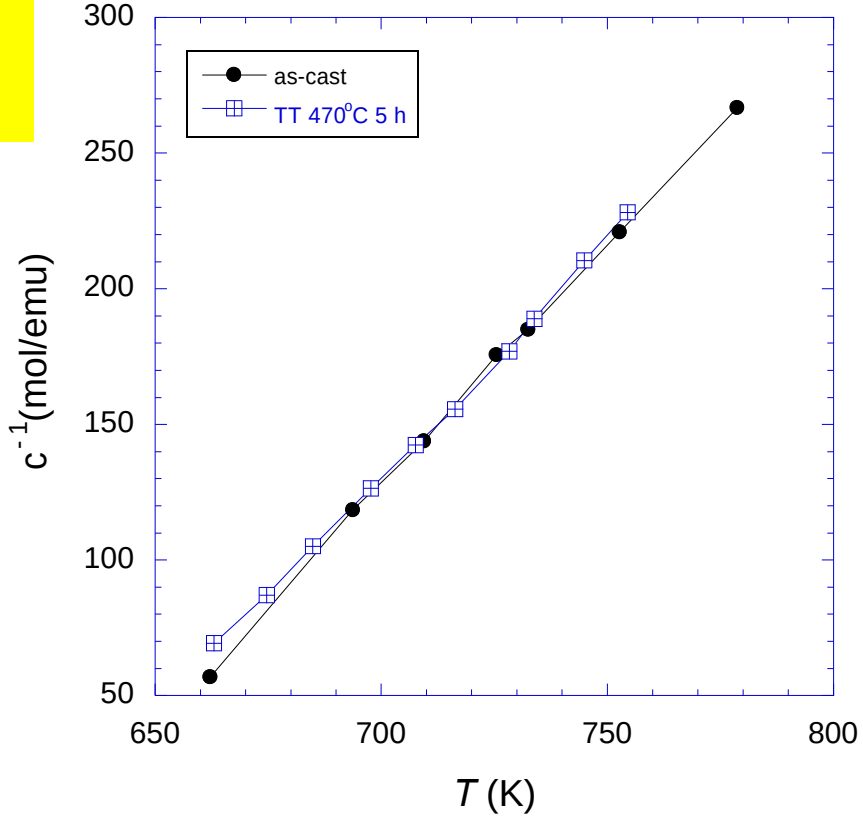

The effective magnetic moments μ_{eff}, the spins S, of the Mn atoms, the τ-phase content c., the average Mn moments in the ordered state μ_{exp}, the paramagnetic Curie temperatures θ, and the Curie temperatures T_C, of the τ-phase of the $Mn_{50}Al_{46}Ni_4$ alloy.

Sample	μ_{eff} /Mn (μ_B)	S_{Mn}	c_τ (%)	μ_{exp} (μ_B)	θ (K)	T_C (K)
As-cast $Mn_{50}Al_{46}Ni_4$	2.98	1.07	35	2.06	629	624
$Mn_{50}Al_{46}Ni_4$ annealed at 470 °C for 5h	3.04	1.1	43	2.09	624	635

S1 P42

Electronic and Magnetic Properties of $Mn_{50}Al_{46}M_4$ (M = Mn, Ni, Ti) Alloys

R. Gavrea [1], S. Mican [1], D. Benea [1], B. Neamţu [2], M. Coldea [1] and V. Pop [1]

[1] Faculty of Physics, Babeş-Bolyai University, Cluj-Napoca, RO-400084 Romania
[2] Materials Science and Engineering Department, Technical University of Cluj-Napoca, RO-400641 Romania

Abstract: In this study we present the results of electronic structure calculations and the experimental investigations on the structural and magnetic properties of the $Mn_{50}Al_{46}M_4$ (M = Mn, Ni, Ti) alloys. The highest magnetic moment was found for the $Mn_{50}Al_{46}Ni_4$ alloy. Total energy calculations point to a more stable antiferromagnetic configuration of the Mn^{1a}-Mn^{2e} pair. DTA measurements pointed out the formation of the metastable τ phase around 470 °C and its decomposition into the stable γ_2 and β-Mn(Al) phases at 850 °C. The τ phase was found along with the ε' phase only in the as-cast sample and the ones annealed at 470°C. A maximum τ phase concentration of 50% was found for the sample annealed at 470 °C for 6 h. The close values of the theoretical and experimental effective magnetic moments confirm the existence of the ε' and τ phases in these alloys.

Experimental and Computational Details:

- Electronic structure calculations were performed in the framework of the Local Density Approximation (LDA) of the Density Functional Theory by means of the SPR-KKR method using the experimentally determined lattice parameters for $Mn_{54}Al_{46}$ (a = 3.94 Å, c = 3.58 Å). All relativistic effects have been taken into account, including the spin-orbit coupling, in the ferromagnetic (FM) and antiferromagnetic (AFM) spin configurations of the Mn^{1a}-Mn^{2e} pair.
- The $Mn_{54}Al_{46}$ and $Mn_{50}Al_{46}Ni_4$ ingots were prepared by induction melting of the starting components under a purified Ar atmosphere.
- The samples were annealed in an inert Ar atmosphere at temperatures between 470 and 850 °C for different times followed by quenching in water.
- XRD investigations were performed using a Brüker D8 Advance X-ray diffractometer with Cu K_α radiation.
- Differential thermal analysis (DTA) was performed between 100 and 900 °C under Ar atmosphere with a temperature ramp rate of 20 °C/min.
- The magnetization and magnetic susceptibility were measured with a Weiss-type magnetic balance in a temperature range of 300-800 K.

Electronic Structure Calculation Results:

Mn-Al system → ***Mn and Al atoms are situated in alternating planes*** spaced at a distance of $c/2$ [1].

Mn atoms situated in ***adjacent planes*** (Mn^{1a}-Mn^{2e} pairs) → ***AFM coupling.***

In order to ***decrease*** the weight of the ***AFM interactions*** → ***Ni or Ti substitutions*** for Mn in $Mn_{54}Al_{46}$.

Smaller Ni or Ti moments → ***increase*** of the ***total magnetic moment*** for $Mn_{50}Al_{46}M_4$ (M = Ni, Ti).

- ***Smaller total energy*** for a ***mixed*** 1a and 2e ***Ni occupancy*** than for an exclusive 2e Ni occupancy.
- ***A lower total energy*** was found for the alloy with the ***AFM coupled Mn^{1a}-Mn^{2e} pair.***

Calculated magnetic moments for the τ phase of $Mn_{50}Al_{46}M_4$(M = Ni, Ti), $Mn_{50}Al_{50}$ and $Mn_{54}Al_{46}$ alloys.

		Mn		Al		M		Total	
		$m_s(\mu_B)$	$m_l(\mu_B)$	$m_s(\mu_B)$	$m_l(\mu_B)$	$m_s(\mu_B)$	$m_l(\mu_B)$	$m_s(\mu_B)$	$m_l(\mu_B)$
$Mn_{50}Al_{50}$		2.41	0.04	-0.08	-	-	-	4.68	0.08
$Mn_{54}Al_{46}$ (FM)	Mn^{2e}	2.43	0.007	-0.08	-	-	-	5.02	0.07
	Mn^{1a}	2.39	0.04						
$Mn_{54}Al_{46}$ (AFM)	Mn^{2e}	-3.17	-0.01	-0.07	-	-	-	4.38	0.08
	Mn^{1a}	2.35	0.04						
$Mn_{50}Al_{46}Ti_4$		2.34	0.04	-0.08	-	-0.66	-0.004	4.43	0.07
$Mn_{50}Al_{46}Ni_4$		2.45	0.04	-0.08	-	0.63	0.06	4.85	0.08

Experimental Results:

During the formation of the τ phase, the following transformation occurs [1,2]:
ε (disordered hexagonal) → ε' (ordered orthorhombic) → τ (tetragonal)

The ***ε' phase*** is an ***ordered ε phase*** [1,2] → ***XRD peaks*** of these two phases ***superimpose.***
Magnetic measurements can ***confirm*** whether the phase is ε or ε'.

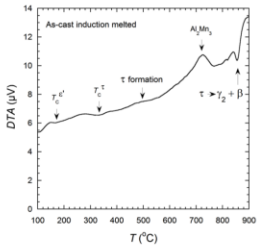

DTA curve for the as-cast $Mn_{50}Al_{46}Ni_4$ alloy.

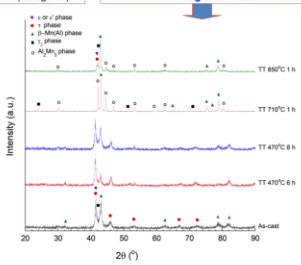

XRD patterns for the $Mn_{50}Al_{46}Ni_4$ alloy after annealing at different temperatures.

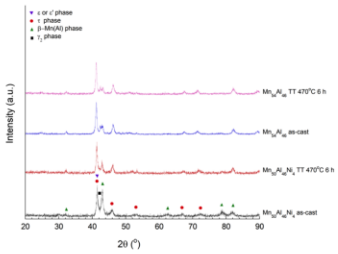

XRD patterns for the as-cast and annealed $Mn_{54}Al_{46}$ and $Mn_{50}Al_{46}Ni_4$ alloys.

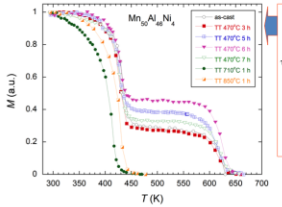

Temperature dependence of the normalized magnetization of the $Mn_{50}Al_{46}Ni_4$ alloy after annealing at different temperatures.

As-cast + TT 470 °C 6h
↓
Two magnetic phases:
τ (hight T_c) and ε' (low T_c).

TT 710 °C + 850 °C
↓
single magnetic phase behavior (lower T_c)

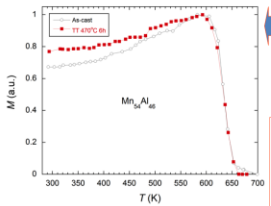

Temperature dependence of the normalized magnetization of the as-cast $Mn_{54}Al_{46}$ alloy and the sample annealed at 470°C for 6 h.

$Mn_{54}Al_{46}$ samples
↓
single magnetic phase behavior (τ phase).

The experimental data fits the Curie-Weiss law $\chi = C/(T-\theta)$ with the parameters given in the table below.

The average experimental Mn moment in the ordered state was calculated taking into account the concentrations c_ε and c_τ of the ε' and τ phases and the theoretical values of Mn moments in the two phases (μ_ε = 1.88 μ_B/Mn atom and μ_τ = 2.37 μ_B/Mn atom [1]) according to the relation: $\mu_{exp} = c_\varepsilon \cdot \mu_\varepsilon + c_\tau \mu_\tau$.

The μ_{eff} values, the Mn spins S, the τ phase content c_τ, the average Mn moments in the ordered state μ_{exp} and μ_{theor}, the paramagnetic Curie temperatures θ, and the Curie temperatures T_c, of the τ phase of the $Mn_{50}Al_{46}Ni_4$ and $Mn_{50}Al_{46}$ alloys.

Sample	μ_{eff}/at	μ_{eff}/Mn (μ_B)	S_{Mn}	c_τ (%)	c_τ (μ_B)	μ_{theor} (μ_B)	μ_{exp} (μ_B)	θ (K)	T_c (K)
$Mn_{50}Al_{46}Ni_4$ as-cast	2.11	2.98	1.07	35	2.14	2.05	629	624	
$Mn_{50}Al_{46}Ni_4$ TT 470 °C 3 h	2.10	2.97	1.07	33	2.14	2.04	617	625	
$Mn_{50}Al_{46}Ni_4$ TT 470 °C 5 h	2.15	3.04	1.1	43	2.2	2.09	624	635	
$Mn_{50}Al_{46}Ni_4$ TT 470 °C 6 h	2.15	3.04	1.1	50	2.2	2.13	633	632	
$Mn_{50}Al_{46}Ni_4$ TT 470 °C 7 h	2.10	2.97	1.07	38	2.14	2.07	625	629	
$Mn_{54}Al_{46}$ as-cast	2.40	3.27	1.21	100	2.42	2.37	662	643	
$Mn_{54}Al_{46}$ TT 470 °C 6 h	2.47	3.36	1.25	100	2.50	2.37	655	644	

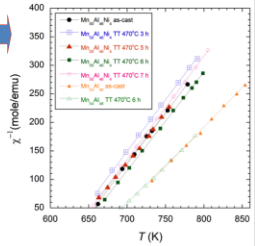

Reciprocal susceptibility versus temperature curves of the $Mn_{50}Al_{46}Ni_4$ and $Mn_{54}Al_{46}$ alloys. The lines represent the Curie-Weiss fit of the experimental data.

Close values of the μ_{theor} and μ_{exp} values ***confirm*** the existence of the ***ε' and τ phases*** in the investigated $Mn_{50}Al_{46}Ni_4$ alloy.

Conclusions:

- The ***largest calculated*** magnetic ***moment*** was found for the ***$Mn_{50}Al_{46}Ni_4$*** alloy.
- A ***lower total energy*** was found for the alloy with the ***AFM coupled Mn^{1a}-Mn^{2e} pair.***
- All of the samples are phase mixtures and are ferromagnetic at room temperature. The ***τ phase was found along with the ε' phase*** only in the ***as-cast $Mn_{50}Al_{46}Ni_4$ sample*** and the ones ***annealed at 470 °C*** with a ***maximum τ phase concentration of 50%.***
- ***Close values of the μ_{theor} and μ_{exp}*** values ***confirm the existence of the ε' and τ phases*** in the investigated $Mn_{50}Al_{46}Ni_4$ alloy.
- Ongoing experimental work is currently being conducted to obtain the τ phase as a majority phase in these compounds.

[1] J. H. Park, Y. K. Hong, S. Bae, J. J. Lee, J. Jalli, G. S. Abo, N. Neveu, S. G. Kim, C. J. Choi, J. G. Lee, *J. Appl. Phys.*, **107**, 09A731 (2010).
[2] T. E. Prost, " PhD Thesis: Magnetic Properties Study of the Mn-Al System with Additions of B or C and Mechanical Milling Techniques", University of Nebraska – Lincoln, 2012.

Acknowledgment
This work was supported by the Romanian Ministry of Education and Research, Grant No. PN-II-ID-PCE-2012-4-0470.

Outline

- Introduction
- MnBi magnetic phase
- MnAl magnetic phase
- **Nanocomposites magnets=Spring magnets**
- Conclusions

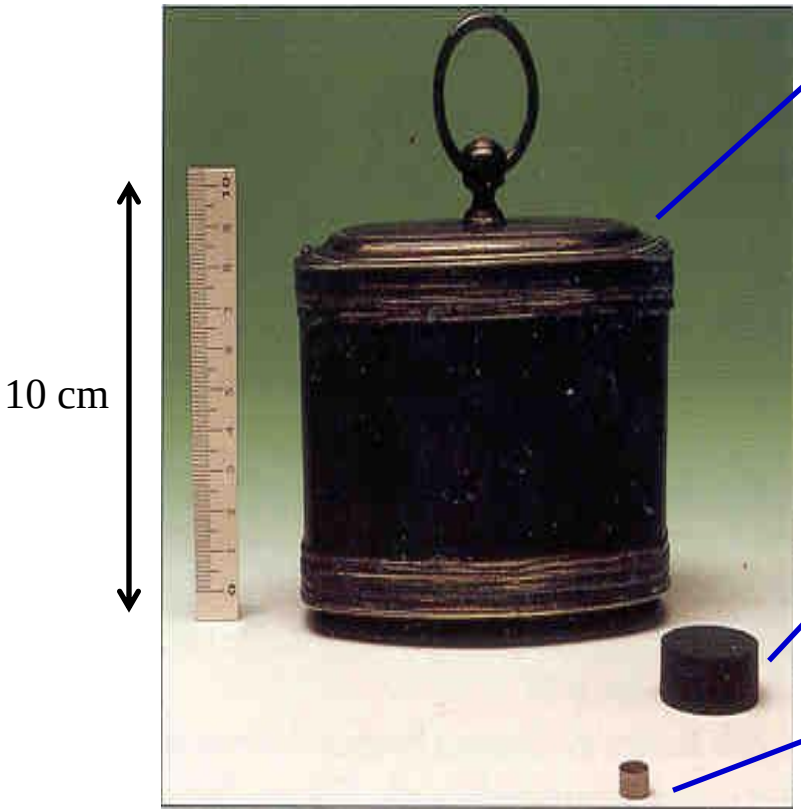

a magnetit magnet (1750)

A ferrite magnet (1940)

rare earth based magnet (1980)

exchange-spring magnets (20??)

All this magnets have the same energy !

Nanophased materials behave differently from their macroscopic counterparts because **their characteristic sizes** are **smaller than the characteristic length scales** of physical phenomena occurring in bulk materials.

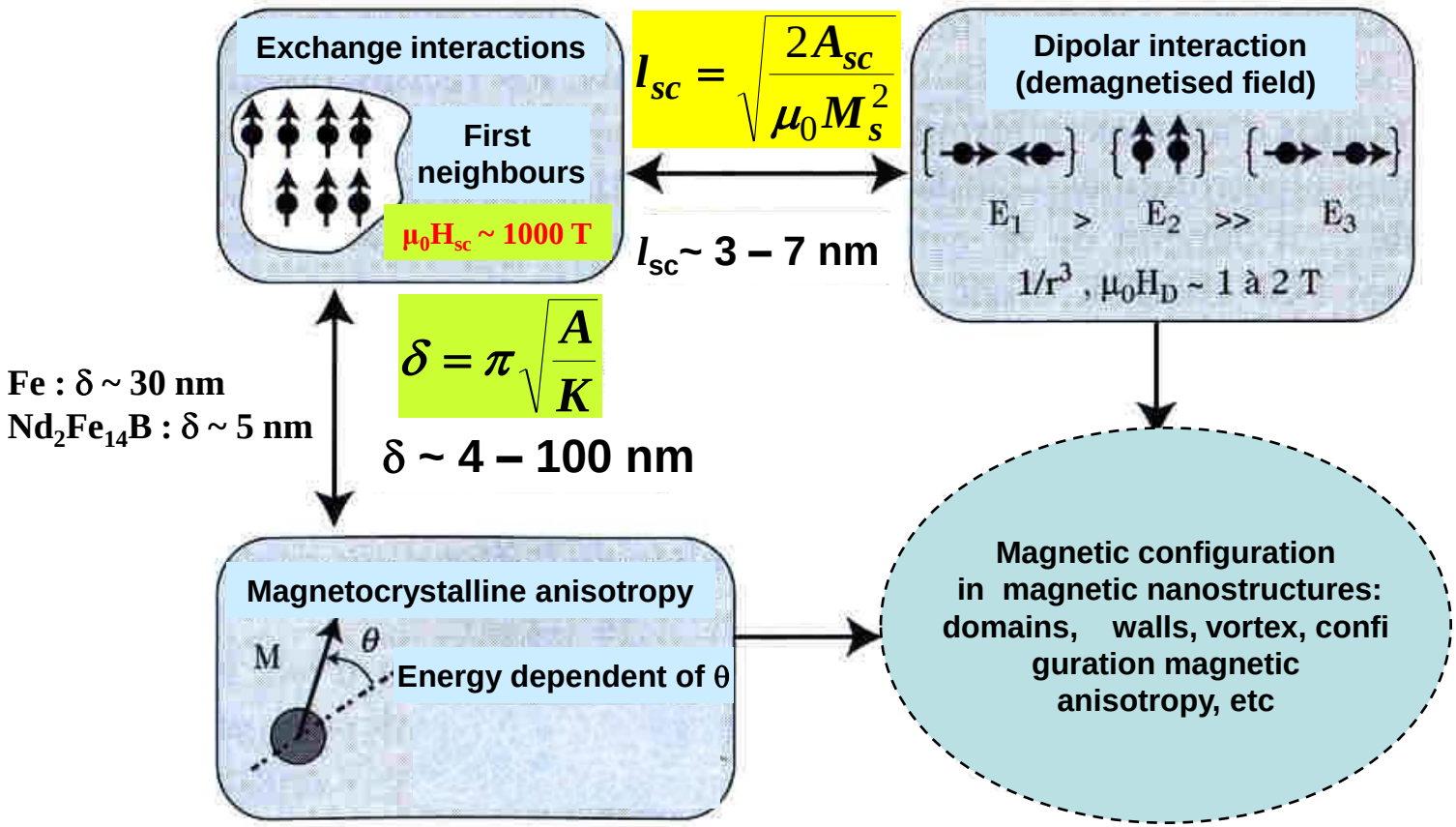

E. De Lacheisserie (edit.), Magnetisme, Presses Universitaires de Grenoble, 1999.

Theoretical predictions:

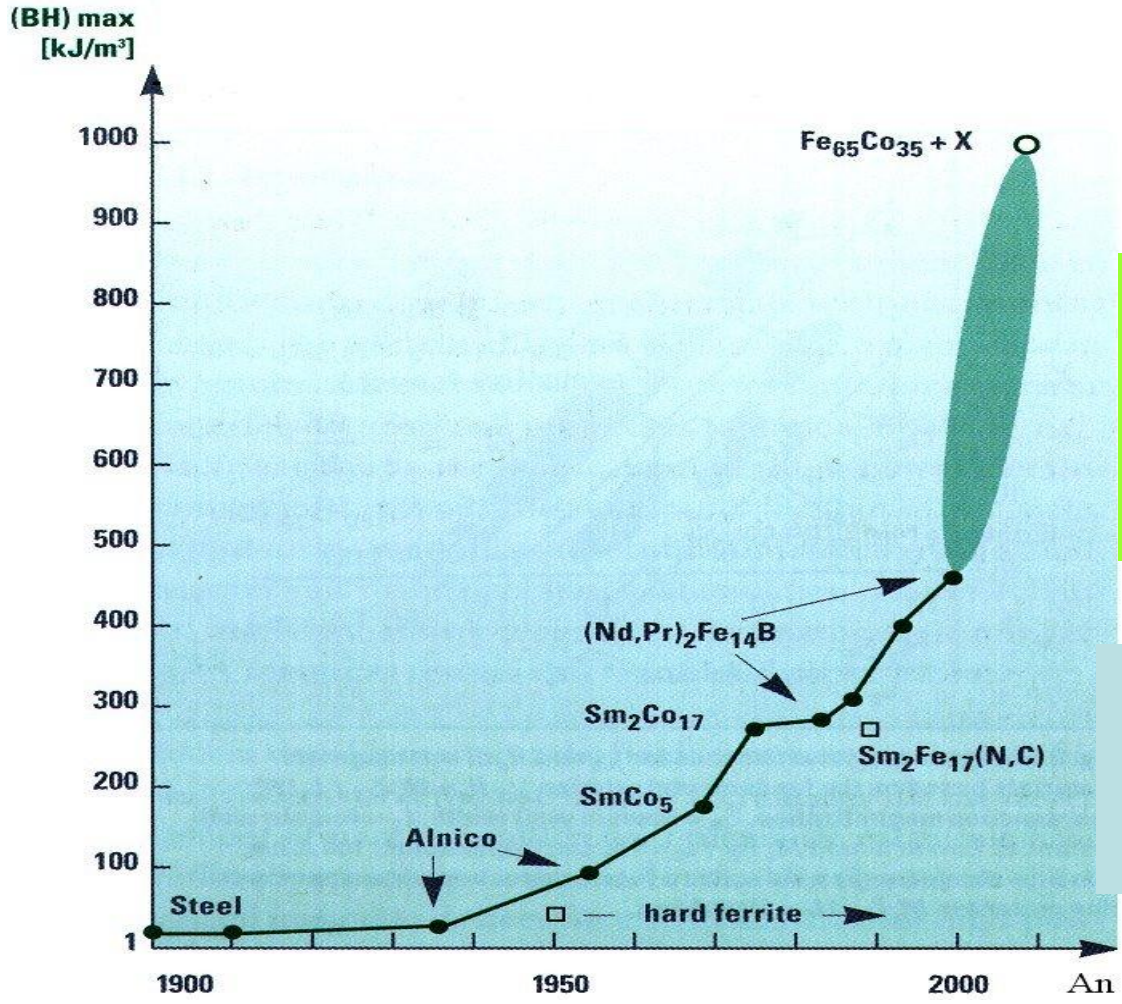

Best magnets on the market:
(BH)max ≈ 500 kJ/m3

$(BH)_{max}$ = 1090 kJ/m^3 for nanostructured multilayers $Sm_2Fe_{17}N_3/Fe_{65}Co_{35}$

R. Skomski, J. Appl. Phys. 76 (1994) 7059

Kronmuller & Coey *Magnetic Materials*, in *European White book on Fundamentel Research in Materials Science* Max Planck Inst. Metallforschung, Stuttgart, 2001, 92-96

Experimental realisations: ??????????

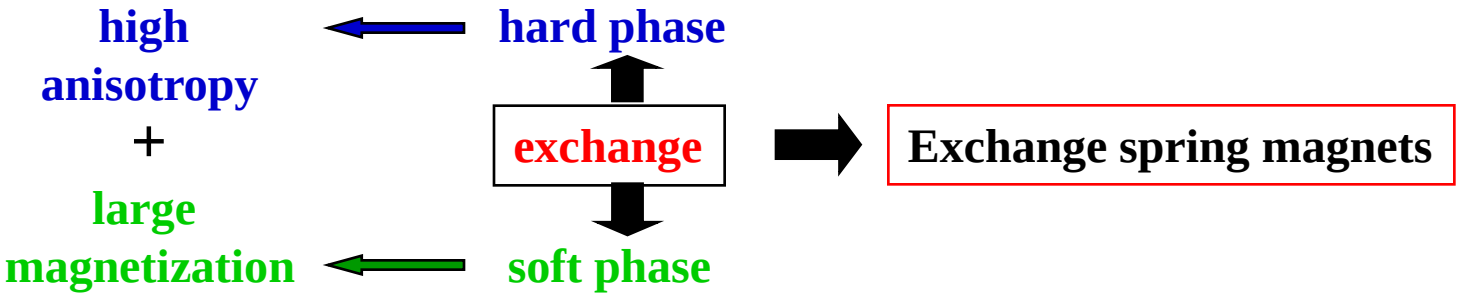
high
anisotropy
+
large
magnetization
hard phase
exchange
soft phase
Exchange spring magnets

Structure
Microstructure → **Soft-hard exchange hardness**

high anisotropy + **large magnetization** → **hard phase**

exchange → **Exchange spring magnets**

soft phase → **exchange**

$$D_{cr} \approx 2\delta_h$$

$$\delta_h = \pi\sqrt{A_h / K_h}$$

D_{cr} = **soft phase critical dimension**

δ_h = width of domain wall in the hard phase

A_h and K_h are the exchange and anisotropy constants

$SmCo_5/\alpha$-Fe Core-Shell Nanocomposite Magnet

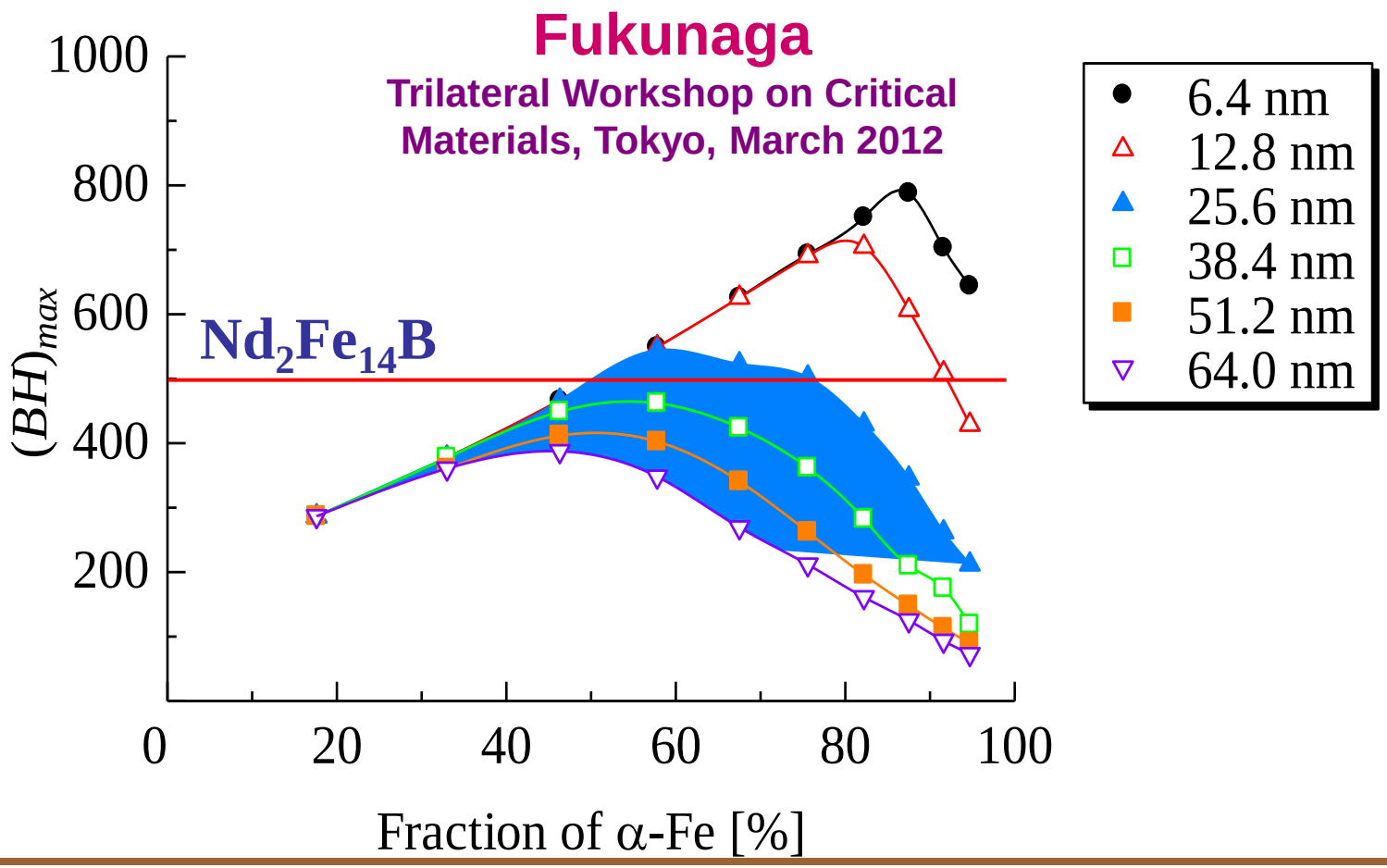

✧ **Fukunaga predicted a drastic increase in $(BH)_{max}$ of $SmCo_5/\alpha$-Fe as a function of α-Fe fraction. The Dresden Group (Neu et al) obtained similar results in SmCo5/Fe multilayers (Intermag 2012). Very recently Hono's Group fabricated Fe/Nd-Fe-B multilayers with $(BH)_m$=61 MGOe (Advanced Materials, 2012).**

IEEE TRANS. MAGN., 48 (2012) 3599,
V. Neu , S. Sawatzki , M.Kopte , Ch. Mickel , and L. Schultz

cross-sectional TEM: $d_{nom}(Fe) = 12$ nm

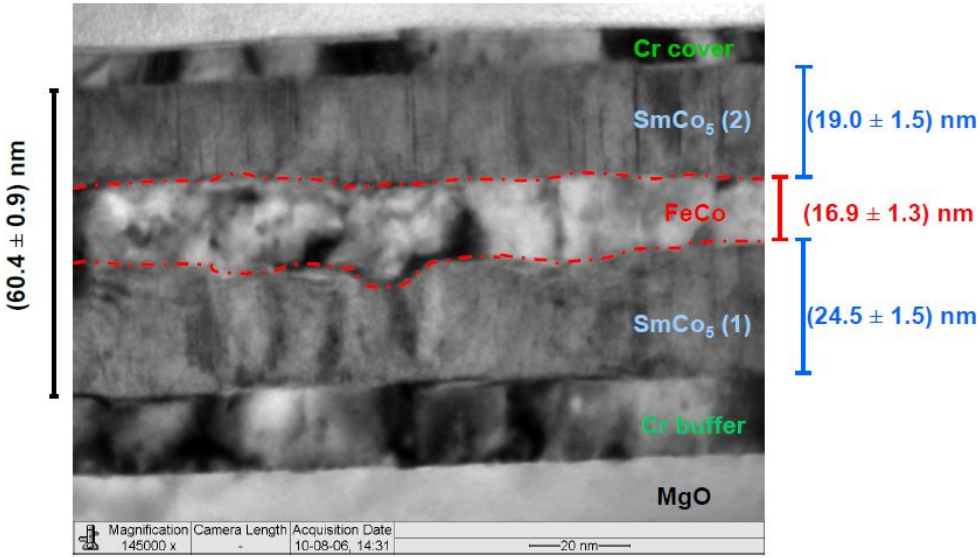

3 layers

5 layers

Ch. Damr

cross-sectional TEM:

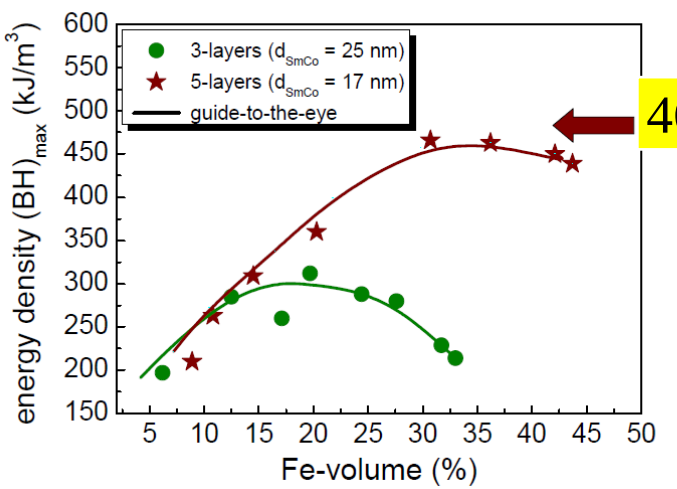

460 kJ/m^3

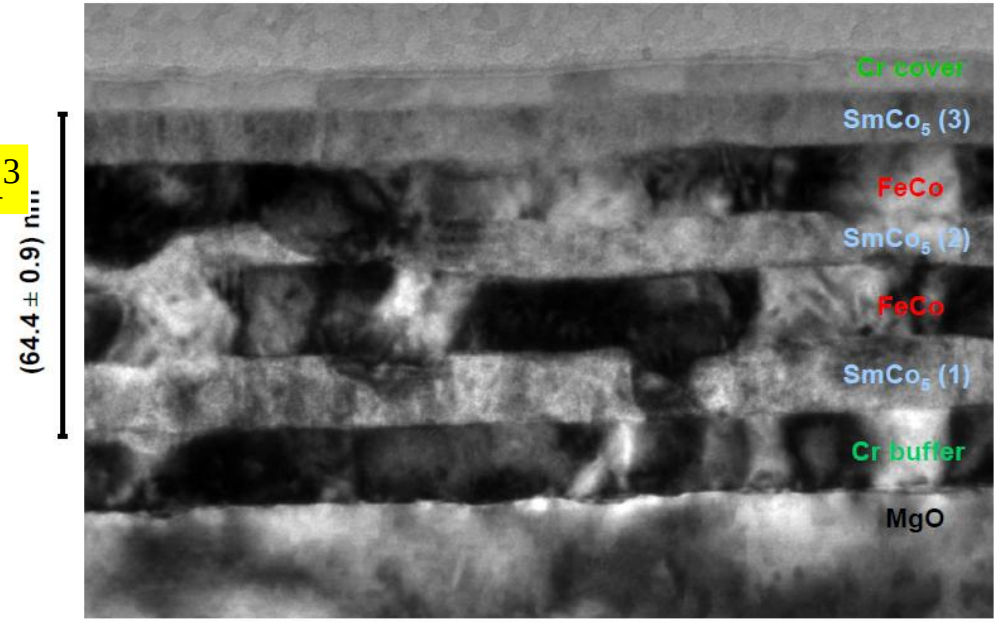

micromagnetic simulations (1)

- code: OOMMF, version 1.2
- 1-dim approach; no x-y discretization
- discretization in z-direction: Δz = 0.5 nm
- intrinsic parameters:

	A (pJ/m)	J_s (T)	K_1 (MJ/m3)
$SmCo_5$	12	1.0	10
Fe	28	2.15	-1.84

- strong coupling at interface: A_i = 20 pJ/m
- geometry: 2 x 25 nm $SmCo_5$ + t_s nm Fe (nominal) or reduced $SmCo_5$ + increased t_s (diffusion)
- field axis: parallel e.a. or tilted (texture)

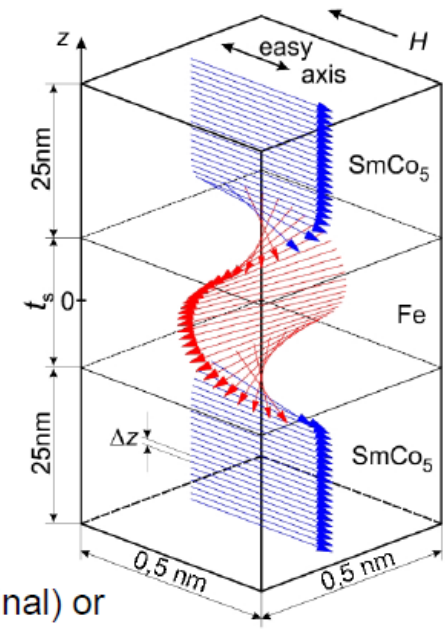

11

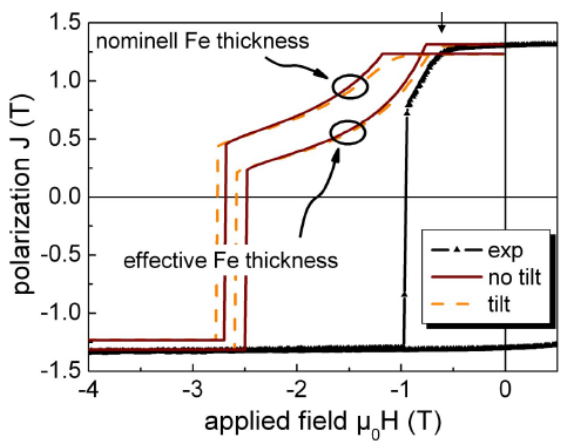

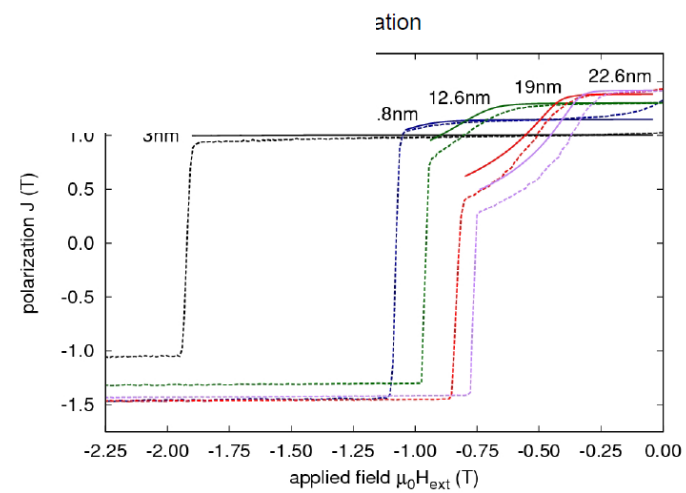

M. Kopte, VN, *et al.* IEEE Trans..Magn. **47** (2011)

Effect of different surfactants on the formation and morphology of $SmCo_5$ nanoflakes*

✓oleylamine (OY),
✓trioctylamine (TOA)
✓oleic acid (OA),

Flake thickness and length, intensity ratio I_{002}/I_{111} values and average grain sizes of the hard $SmCo_5$ phase.

Original powder	Balls	Surfactants	Milling time (h)	Flake thickness (nm)	Flake length (μm)	I_{002}/I_{111}	Average grain size (nm)
$SmCo_5$ ingot after crushed and ground	Mixture of different diameters: Φ4–12 mm	30 wt.% OY	3	20–210	0.5–13	2.5	21
			4	15–170	0.5–11	2.4	16
			5	8–80	0.5–10	1.5	13
			6	8–80	0.2–8	0.6	10
		30 wt.% OA	3	20–210	0.5–13	2.6	21
			4	15–170	0.5–11	2.6	21
			5	8–80	0.5–10	1.8	20
			6	8–80	0.2–8	0.8	15
		30 wt.% TOA	0	–	1–40[a]	–	–
			5	–	0.5–20[a]	2	11
			10	–	0.5–20[a]	–	–
		100 wt.% TOA	2.5	80–300	0.5–10	3.4	21
			5	30–150	0.3–8	2.5	11
		40 wt.% TOA	0.25	–	1–17[a]	22.8	–
			0.5	500–1600	1–17	19.5	–
			1	80–800	1–15	7.2	–
			2	80–420	1–12	4.0	–
			2.5	80–200	1–10	3.8	21
			3	60–180	0.5–10	2.0	21
			4	50–150	0.5–10	1.5	18
			5	30–120	0.5–8	0.8	11
Jet-milled $SmCo_5$	Single diameter: Φ4 mm	5 wt.% OA	0	–	0.5–10[a]	63.6	–
			0.25	–	0.3–10[a]	43.1	–
			0.5	–	0.3–10[a]	22.2	–
			1	20–350	0.5–10	16.5	–
			2	10–200	0.4–10	4.3	–
			5	8–150	0.3–10	1.4	9
		2 wt.% OA	5	10–210	0.3–10	0.4	9
		5 wt.% OA	5	8–150	0.3–10	1.4	9
		10 wt.% OA	5	5–100	0.3–10	2.0	9

[a] Particle size.

* Liyun Zheng, Baozhi Cui, George C. Hadjipanayis, Acta Materialia 59 (2011) 6772–6782

Effect of different surfactants on the formation and morphology of $SmCo_5$ nanoflakes*

✓oleylamine (OY),
✓trioctylamine (TOA)
✓oleic acid (OA),

Flake thickness and length, intensity ratio I_{002}/I_{111} values and average grain sizes of the hard $SmCo_5$ phase.

Original powder | Balls

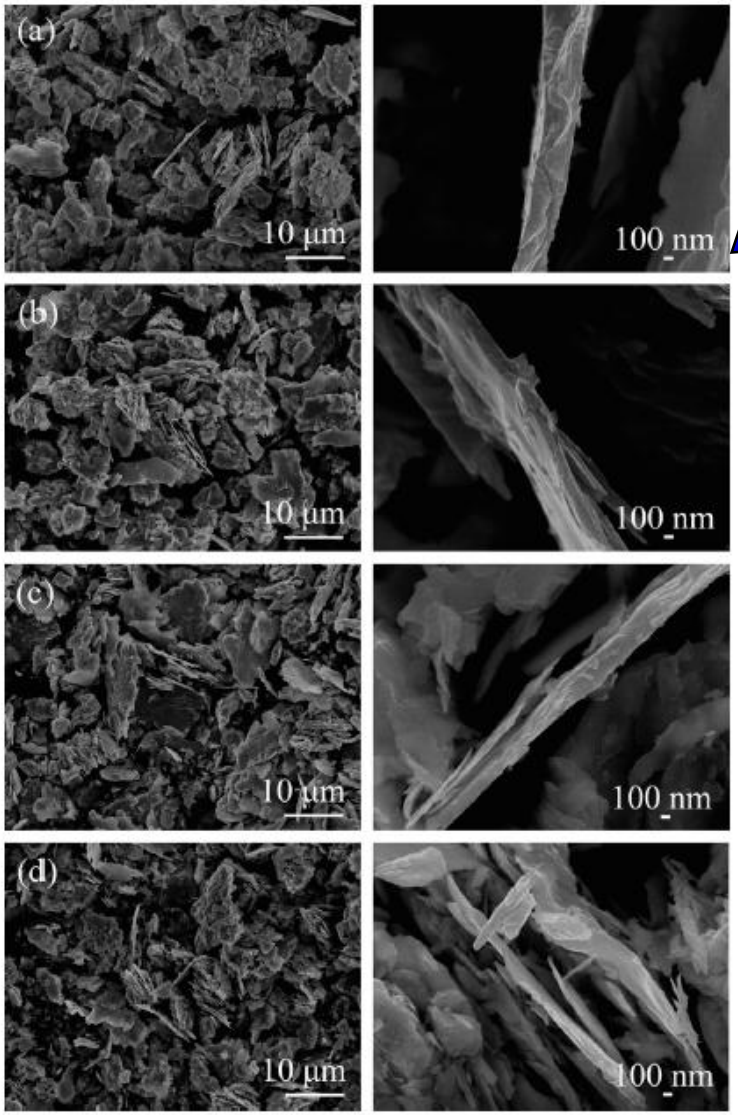

Surfactants	Milling time (h)	Flake thickness (nm)	Flake length (μm)	I_{002}/I_{111}	Average grain size (nm)
30 wt.% OY	3	20–210	0.5–13	2.5	21
	4	15–170	0.5–11	2.4	16
	5	8–80	0.5–10	1.5	13
	6	8–80	0.2–8	0.6	10
[illegible] % OA	3	20–210	0.5–13	2.6	21
	4	15–170	0.5–11	2.6	21
	5	8–80	0.5–10	1.8	20
	6	8–80	0.2–8	0.8	15
30 wt.% TOA	0	–	1–40[a]	–	–
	5	–	0.5–20[a]	2	11
	10	–	0.5–20[a]	–	–
100 wt.% TOA	2.5	80–300	0.5–10	3.4	21
	5	30–150	0.3–8	2.5	11
40 wt.% TOA	0.25	–	1–17[a]	22.8	–
	0.5	500–1600	1–17	19.5	–
	1	80–800	1–15	7.2	–
	2	80–420	1–12	4.0	–
	2.5	80–200	1–10	3.8	21
	3	60–180	0.5–10	2.0	21
	4	50–150	0.5–10	1.5	18
	5	30–120	0.5–8	0.8	11
5 wt.% OA	0	–	0.5–10[a]	63.6	–
	0.25	–	0.3–10[a]	43.1	–
	0.5	–	0.3–10[a]	22.2	–
	1	20–350	0.5–10	16.5	–
	2	10–200	0.4–10	4.3	–
	5	8–150	0.3–10	1.4	9
2 wt.% OA	5	10–210	0.3–10	0.4	9
5 wt.% OA	5	8–150	0.3–10	1.4	9
10 wt.% OA	5	5–100	0.3–10	2.0	9

micro-size powders became flakes.

Liyun Zheng, Baozhi Cui, George C. Hadjipanayis, Acta Materialia 59 (2011) 6772–6782

Effect of different surfactants on the formation and morphology of $SmCo_5$ nanoflakes*

✓oleylamine (OY),
✓trioctylamine (TOA)
✓oleic acid (OA),

Flake thickness and length, intensity ratio I_{002}/I_{111} values and average grain sizes of the hard $SmCo_5$ phase.

Original powder	Balls	Surfactants	Milling time (h)	Flake thickness (nm)	Flake length (μm)	I_{002}/I_{111}	Average grain size (nm)
$SmCo_5$ ingot after crushed and ground	Mixture of different diameters: Φ4–12 mm	30 wt.% OY	3	20–210	0.5–13	2.5	21
			4	15–170	0.5–11	2.4	16
			5	8–80	0.5–10	1.5	13
			6	8–80	0.2–8	0.6	10
		30 wt.% OA	3	20–210	0.5–13	2.6	21
			4	15–170	0.5–11	2.6	21
			5	8–80	0.5–10	1.8	20
			6	8–80	0.2–8	0.8	15
		30 wt.% TOA	0	–	1–40[a]	–	–
			5	–	0.5–20[a]	2	11
			10	–	0.5–20[a]	–	–
		100 wt.% TOA	2.5	80–300	0.5–10	3.4	21
			5	30–150	0.3–8	2.5	11
		40 wt.% TOA	0.25	–	1–17[a]	22.8	–
			0.5	500–1600	1–17	19.5	–
			1	80–800	1–15	7.2	–
			2	80–420	1–12	4.0	–
			2.5	80–200	1–10	3.8	21
			3	60–180	0.5–10	2.0	21
			4	50–150	0.5–10	1.5	18
			5	30–120	0.5–8	0.8	11
Jet-milled $SmCo_5$	Single diameter: Φ4 mm	5 wt.% OA	0	–	0.5–10[a]	63.6	–
			0.25	–	0.3–10[a]	43.1	–
			0.5	–	0.3–10[a]	22.2	–
			1	20–350	0.5–10	16.5	–
			2	10–200	0.4–10	4.3	–
			5	8–150	0.3–10	1.4	9
		2 wt.% OA	5	10–210	0.3–10	0.4	9
		5 wt.% OA	5	8–150	0.3–10	1.4	9
		10 wt.% OA	5	5–100	0.3–10	2.0	9

[a] Particle size.

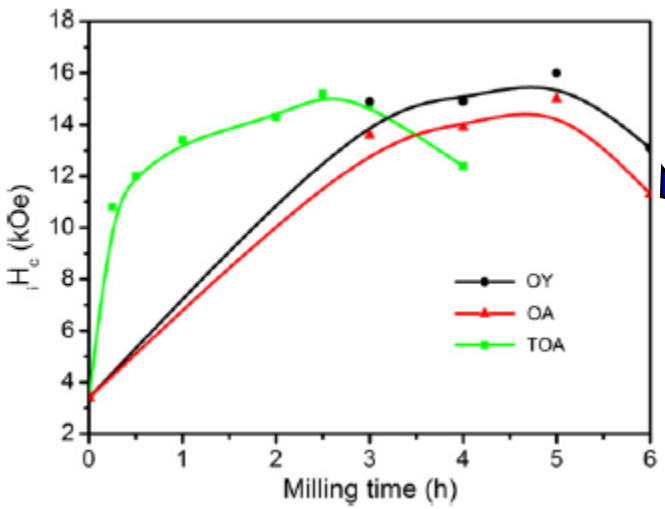

* Liyun Zheng, Baozhi Cui, George C. Hadjipanayis, Acta Materialia 59 (2011) 6772–6782

Our researches

- hard magnetic phases of $SmCo_5$, $SmCo_3Cu_2$, $R_2Fe_{14}B$
- soft magnetic phases of α-Fe, Fe-Co (~20 or 10 wt%)

$SmCo_5$	large anisotropy
$SmCo_3Cu_2$	large coercivity
$R_2Fe_{14}B$	best magnets

Our researches

- hard magnetic phases of $SmCo_5$, $SmCo_3Cu_2$, $R_2Fe_{14}B$
- soft magnetic phases of α-Fe, Fe-Co (~20 or 10 wt%)

$SmCo_5$	large anisotropy
$SmCo_3Cu_2$	large coercivity
$R_2Fe_{14}B$	best magnets

Magnetic Hard/Soft nanocomposites – Spring magnets

($SmCo_5$, $SmCo_3Cu_2$, $R_2Fe_{14}B$)+x% (α-Fe or $Fe_{65}Co_{35}$

- composition, x= 10 or 22 wt % Fe
- milling time
- conventional annealing/short time annealing

Material preparation

- milling of the powders in a high energy planetary mill
- heat treatments (temperatures and duration)

Starting materials :

- **hard magnetic phases**
  ingots – prepared by melting
- **Fe NC 100.24 powder (Höganäs), (< 40 μm) and**
- **$Fe_{65}Co_{35}$ obtained by melting**

Mechanical milling experiments:

- **premilling of hard and soft magnetic ingots**
- **hard magnetic + α-Fe (or $Fe_{65}Co_{35}$)** mixed powders – milled in Ar for **1.5 – 12** h

Annealing:

- **conventional annealing:** **in vacuum/450-650 ° C for 0.5 up to 10 h.**
- **short time annealing:** **in argon/700, 750 or 800 ° C for 0.5 to 3 min.**

Material characterisation

- X-rays diffraction (XRD)
- DSC measurements
- Electron microscopy (SEM and TEM)
  - morphology
  - chemical composition checked by EDX
- Magnetic measurements

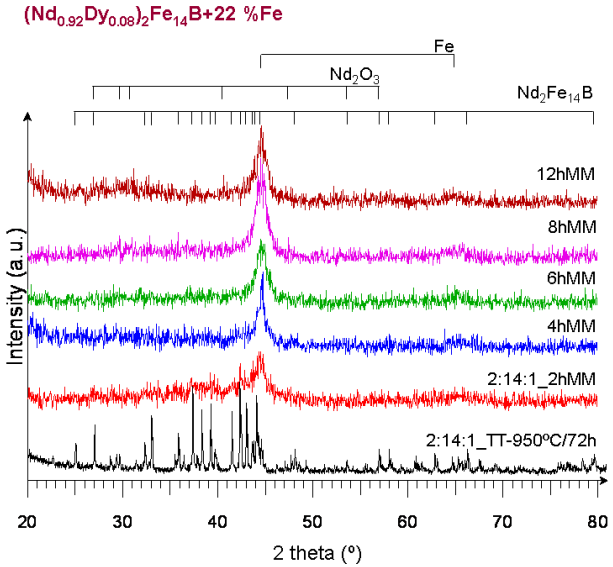
(Nd0.92Dy0.08)2Fe14B+22 %Fe
Fe
Nd2O3
Nd2Fe14B
12hMM
8hMM
6hMM
4hMM
2:14:1_2hMM
2:14:1_TT-950ºC/72h
Intensity (a.u.)
20
30
40
50
60
70
80
2 theta (º)

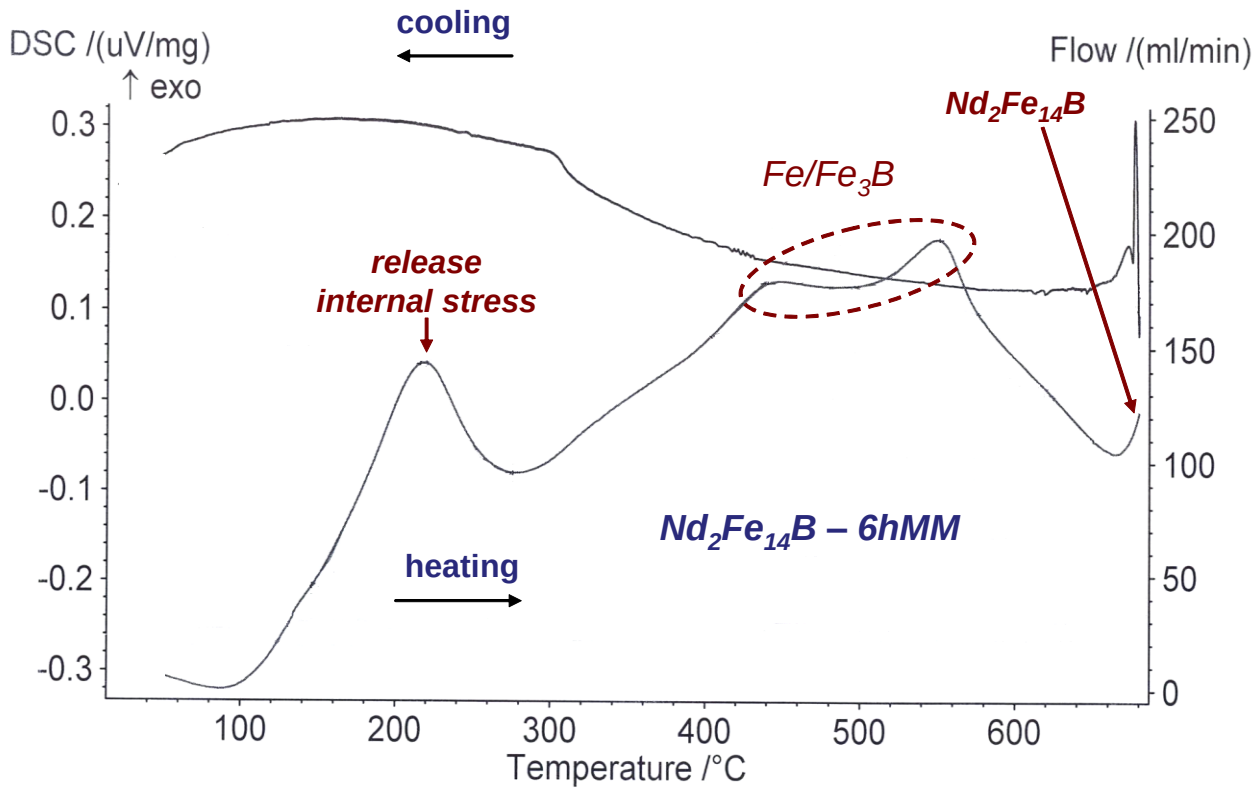
cooling
DSC /(uV/mg)
↑ exo
Flow /(ml/min)
Nd2Fe14B
Fe/Fe3B
release
internal stress
Nd2Fe14B – 6hMM
heating
0.3
0.2
0.1
0.0
-0.1
-0.2
-0.3
250
200
150
100
50
0
100
200
300
400
500
600
Temperature /°C

Classical annealing

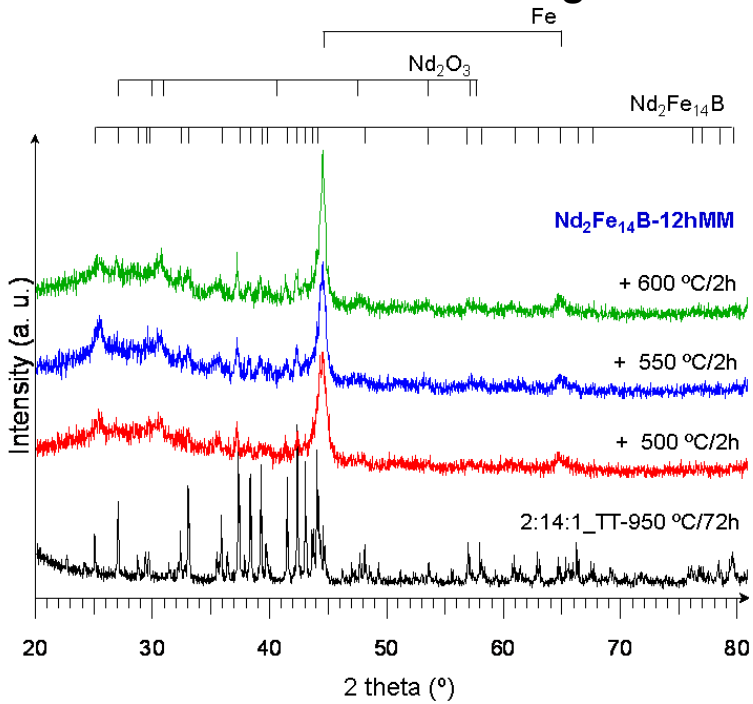

S. Gutoiu, V. Pop et al., J. Optoelectron. Adv. Mater. 12 (2010) 2126-2131

Short time annealing

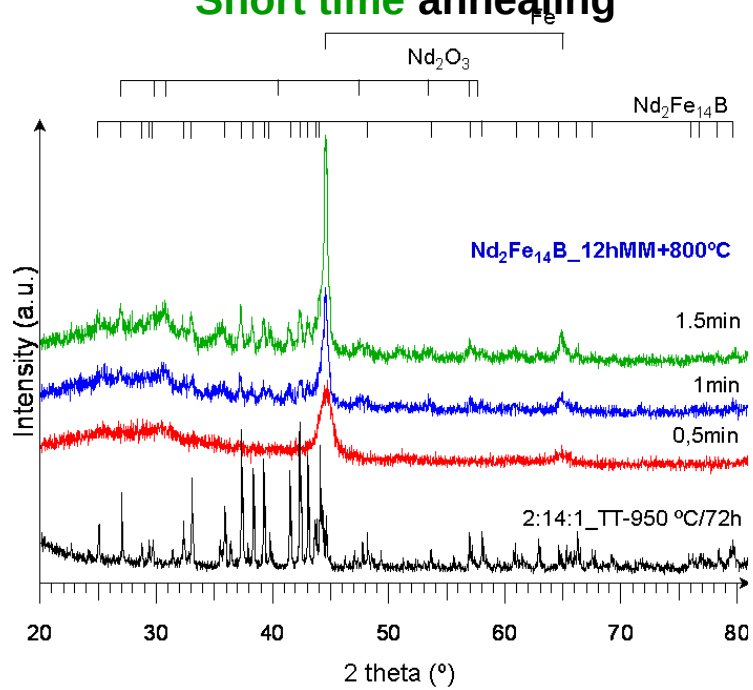

Atomic-Scale Investigation

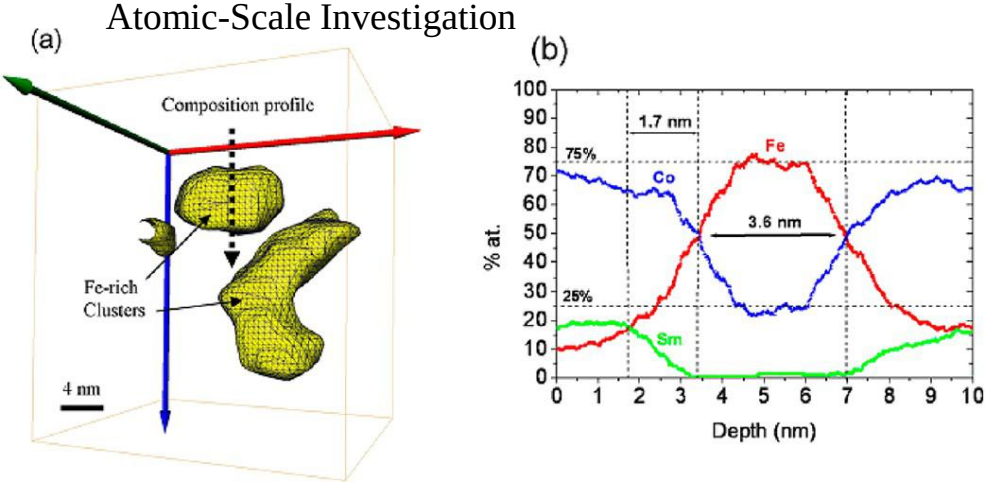

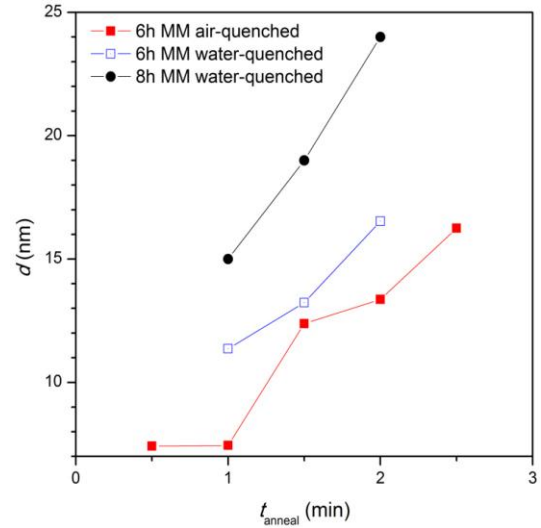

R. Lardé, J-M. Le Breton, A. Maître, D. Ledue, O. Isnard, V. Pop and I. Chicinaş, J. Phys. Chem., 117 (2013) 7801

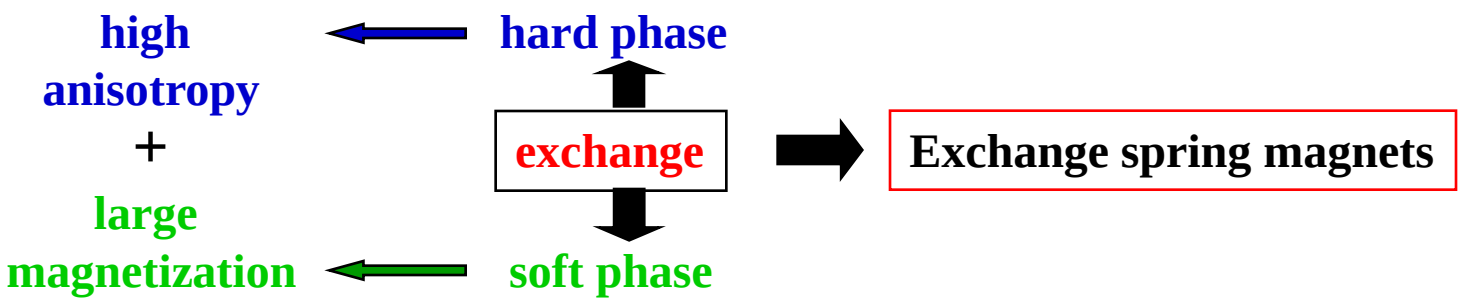
high
anisotropy
+
large
magnetization
hard phase
exchange
soft phase
Exchange spring magnets

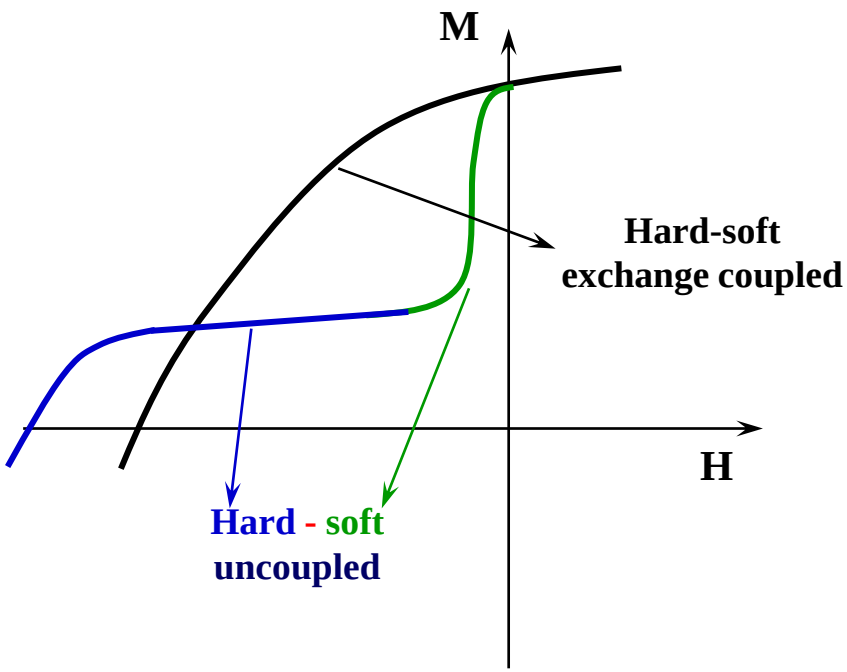
M
H
Hard-soft
exchange coupled
Hard - soft
uncoupled

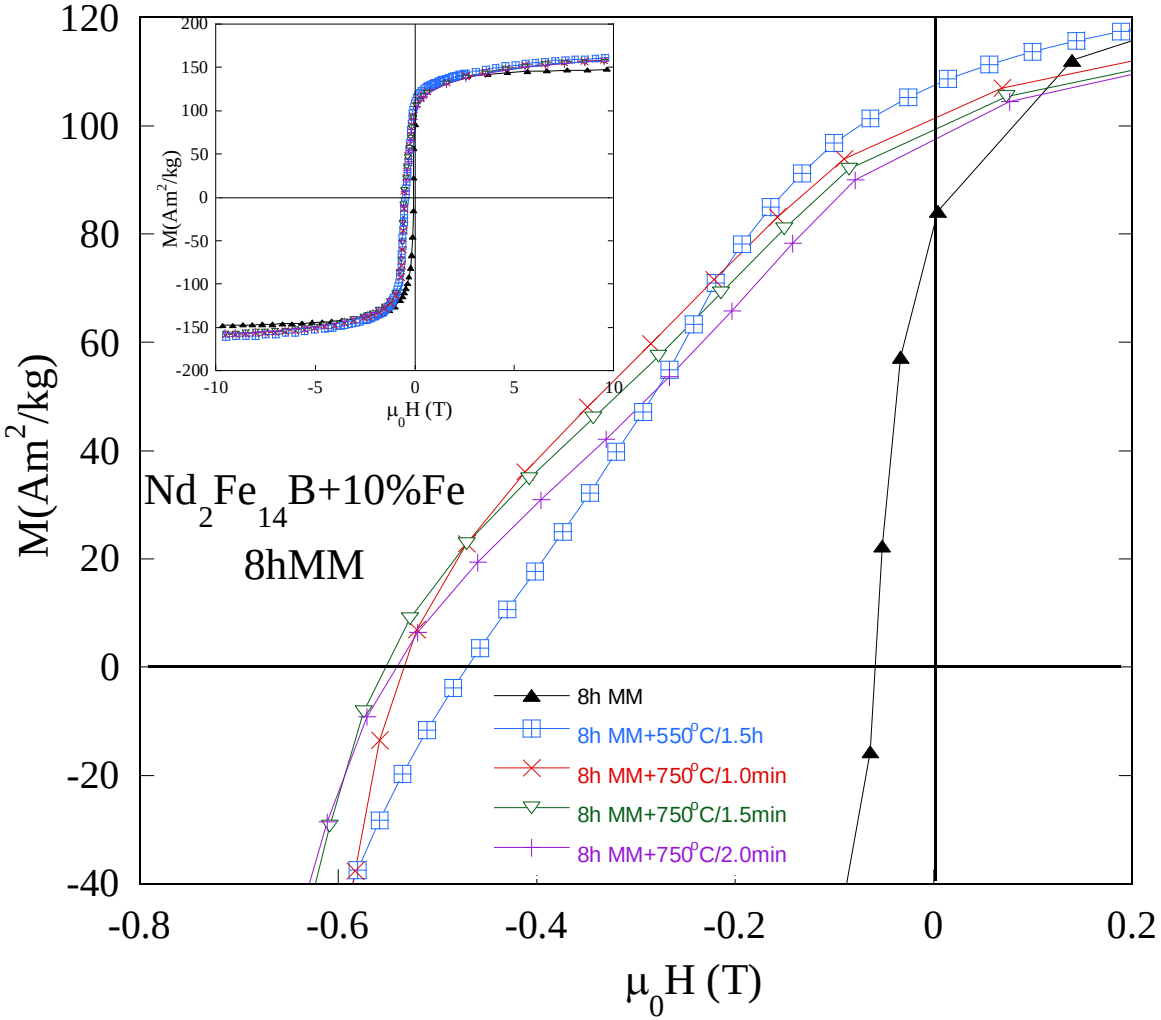

$Nd_2Fe_{14}B$ + 10 % α-Fe; 8h MM

Classical annealing ⟷ **Short time annealing**

H_c- evident increasing

M_r- small decreasing

The influence of the type of hard magnetic phase

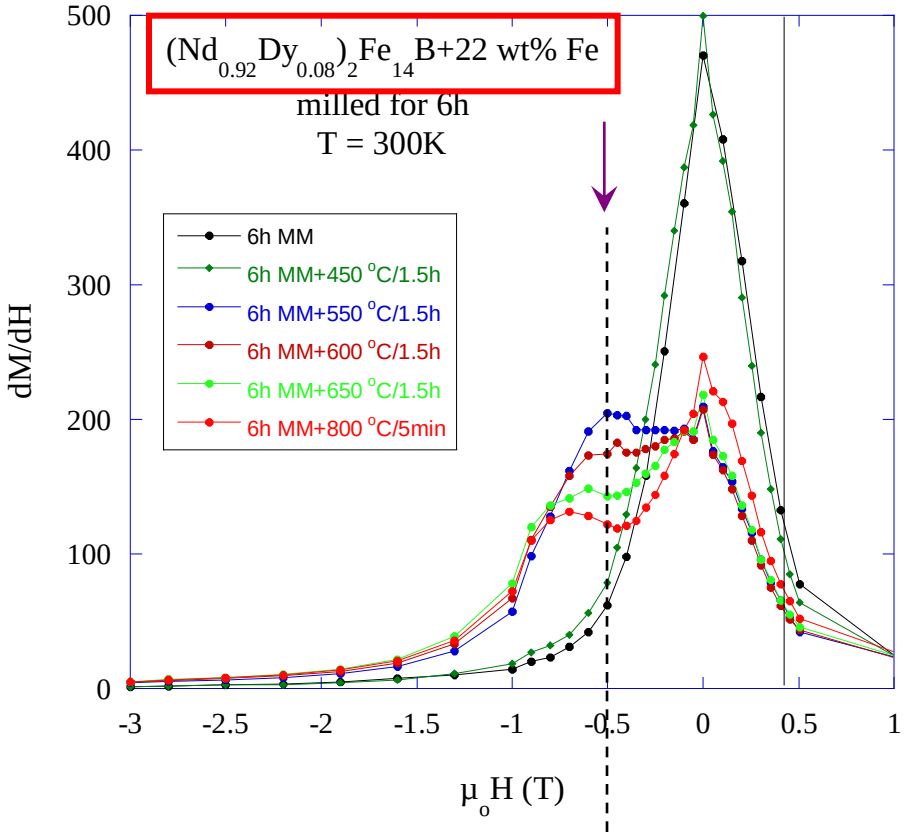

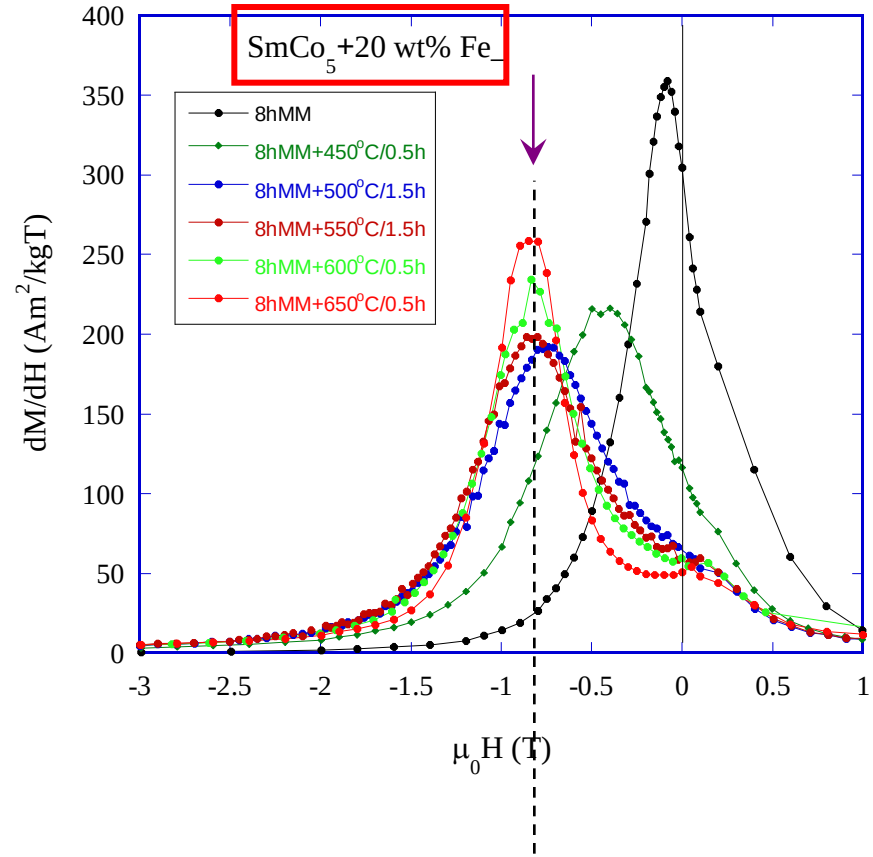

$R_2Fe_{14}B$/Fe

Lower coercivity
Two peaks,
pour hard/soft magnetic coupling

$SmCo_5$/Fe

Higher coercivity
One peak,
good hard/soft magnetic coupling

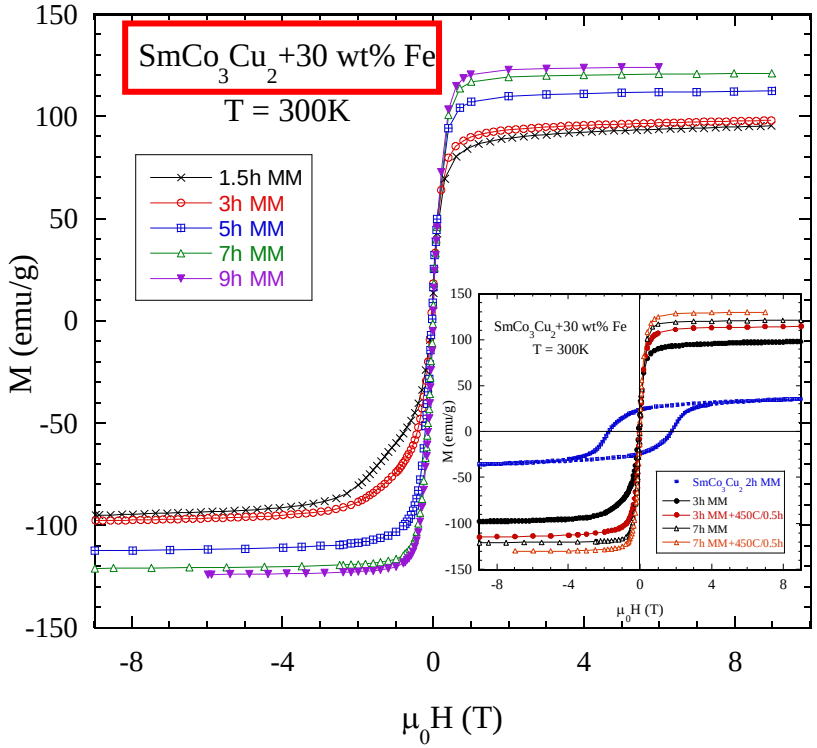

the importance of the
intrinsic anisotropy*

*D. Givord, O. Isnard,, V. Pop, I. Chicinas, JMMM 316 (2007)

This behavior was connected with coercivity mechanism of the $SmCo_3Cu_2$ phase given by the microstructure [1-2] and diminishing of the intrinsic coercivity by Co substitution with Cu [3].

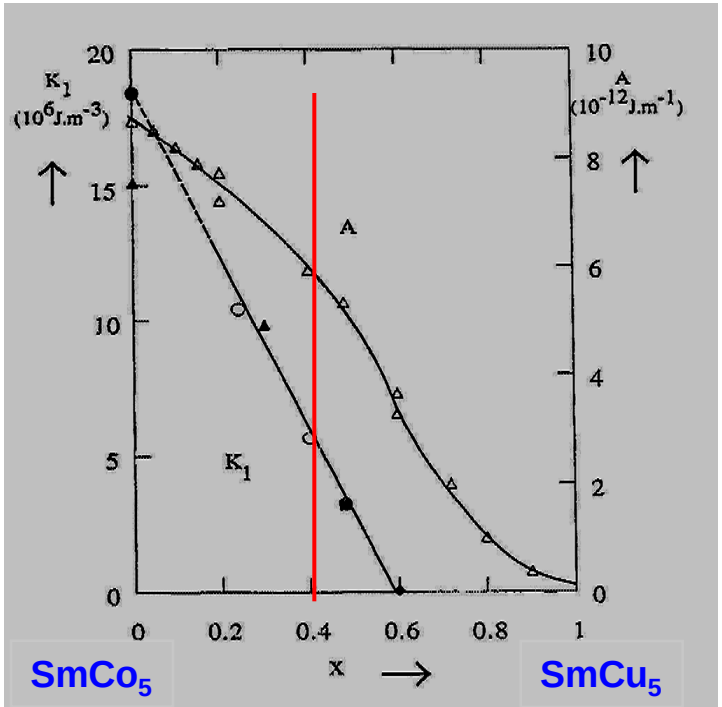

[1] E. Estevez-Rams, J. Fidler, A. Penton, J.C. Tellez-Blanco, R.S. Turtelli, R. Grossinger, J. Alloys Compounds, 283 (1999) 327.

[2] P. Kerschl, A. Handstein, K. Khlopkov, O. Gutfleisch, D. Eckert, K. Nenkov, J.-C. Te´ llez-Blanco, R. Gro¨ ssinger, K.-H. Mu¨ ller, L. Schultz, J. Magn. Magn. Matter. 290–291 (2005) 420.

[3] E. Lectard, C.H. Allibert, R. Ballou, J. Appl. Phys. 75 (1994) 6277.

The influence of the hard/soft ratio

$SmCo_5$+x% Fe (x=20 or 30),

milled 6 and 8 h and annealed at 550° C for 1.5 h*

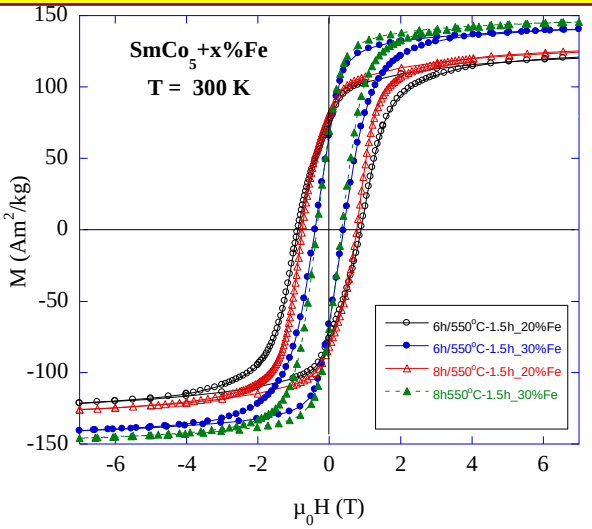

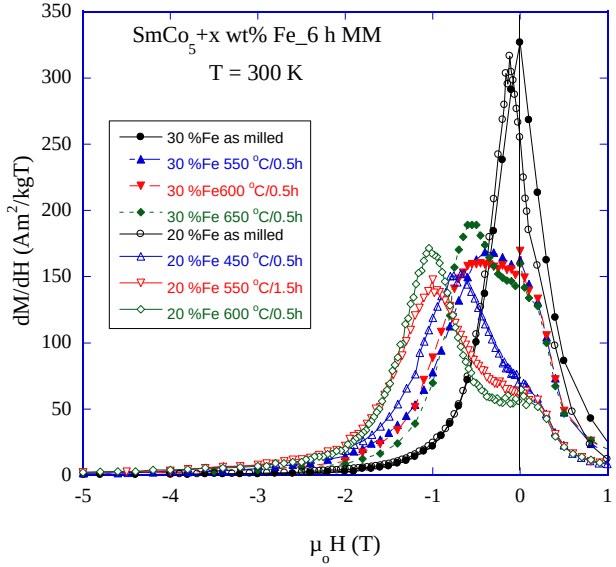

*V. Pop, O. Isnard, D. Givord, I. Chicinas, JMMM 310 (2007) 2489

V. Pop, O. Isnard, D. Givord, I. Chicinas, J. M. Le Breton, JOAM 8 (2006) 494

$Nd_2Fe_{14}B$ + 10 % α-Fe; 8h MM

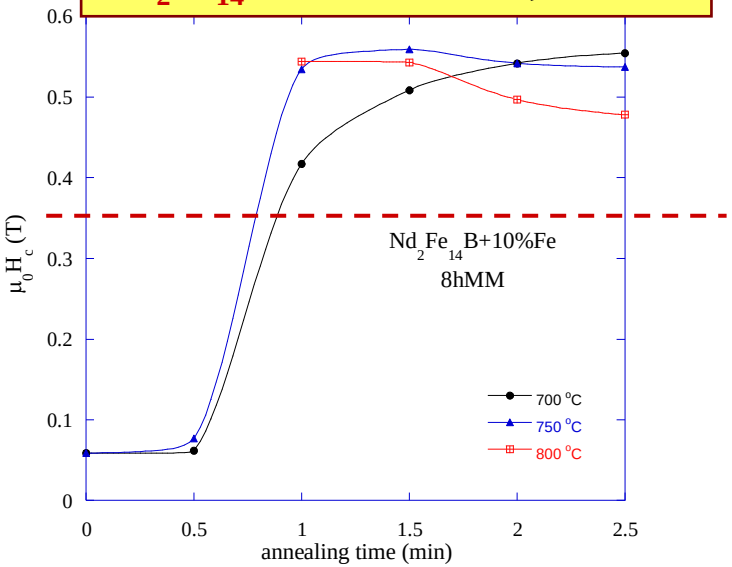

$Nd_2Fe_{14}B$ + 22 % α-Fe; 8h MM

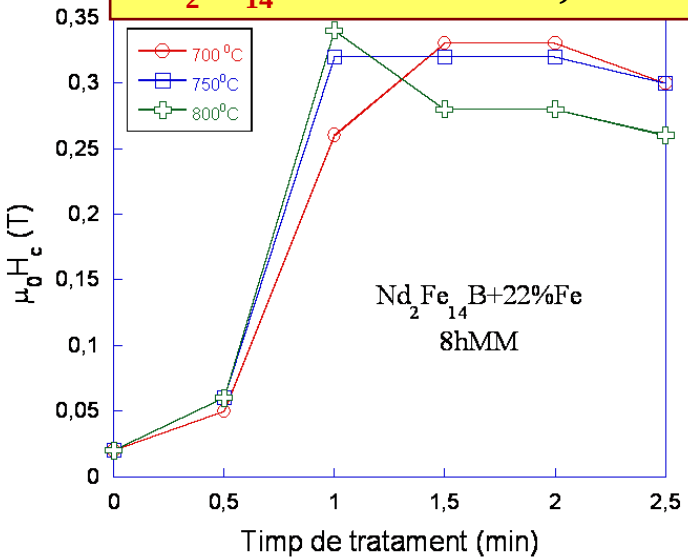

V. Pop et al., J. Alloys Compd. (2011)

V. Pop et al. , J. Alloys Compd. 581 (2013) 821–827

S1 P41

Microstructure and Interphase Magnetic Coupling in $Nd_2Fe_{14}B$/α-Fe Nanocomposites Obtained by Mechanical Milling and Short Time Annealing

S. Mican [1], R. Hirian [1], V. Pop [1], I. Chicinaş [4] and O. Isnard [2,3]

[1] Faculty of Physics, Babeş-Bolyai University, Cluj-Napoca, RO-400084 Romania
[2] Université Grenoble Alpes, Institut Néel, Grenoble, F-38042 France
[3] CNRS, Institut Néel, Grenoble, F-38042 France
[4] Materials Science and Engineering Department, Technical University of Cluj-Napoca, RO-400641 Romania

Abstract: This study presents the effect of different milling times and short time annealing on the structural and magnetic properties of $Nd_2Fe_{14}B$/10wt % Fe nanocomposites prepared by high energy ball milling. The XRD peaks of the hard magnetic phase disappear after milling due to the damaging of the $Nd_2Fe_{14}B$ crystal structure. After annealing, the characteristic peaks of the hard magnetic phase are restored with a limited growth of the soft magnetic phase crystallites. The magnetic behavior was investigated from hysteresis curves and *dM/dH* vs. *H* plots. The best exchange coupling was obtained for the 6 h milled sample annealed at 700 ˚C for 2 minutes with a maximum coercive field value of 0.44 T. Taking into account the milling and annealing conditions, the $Nd_2Fe_{14}B$/α-Fe exchange coupling is analyzed.

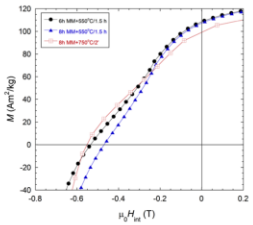

For ***classically annealed samples***, the interphase exchange coupling is better after 6 h MM compared to 8 h MM [1,2]. ***What will happen after short time annealing?***

Experimental:

- The $Nd_2Fe_{14}B$ hard phase was prepared by induction melting in an Ar atmosphere, followed by annealing in vacuum at 950 ˚C for 68 h. The ingot was ground to a fine powder under 500 μm. The soft magnetic phase (12 g of NC 100.24 commercial Fe powder – Höganäs product) was milled with 5 ml benzene for 4 h in an inert Ar atmosphere with a ball to powder weight ratio of 10:1.
- The $Nd_2Fe_{14}B$ powder was mixed with the pre-milled Fe phase in a weight ratio of 90% $Nd_2Fe_{14}B$/10% Fe. The mixture was dry-milled in Ar for 2, 4 and 6 h respectively with a ball to powder weight ratio of 10:1. The milled samples were annealed in an Ar atmosphere at 700, 750 and 800 ˚C for 0.5-2.5 min and quenched in water.
- X-Ray diffraction measurements were performed on a Brüker D8 Advance diffractometer using Cu K_α radiation.
- Magnetic measurements were carried out on powder samples fixed in epoxy resin using the extraction method at 300 K in applied fields up to ±10T. Assuming isolated spherical magnetic particles we used a demagnetization factor of 1/3 for magnetic data.

Results and Discussions:

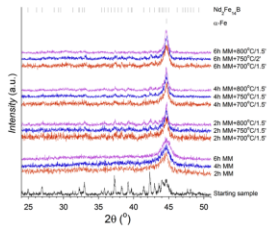

XRD: starting, as-milled and annealed $Nd_2Fe_{14}B$+10%Fe samples.

Damaging of the crystal structure and increased internal stress and defect density by MM.

Hard phase XRD peaks disappear even after 2 h MM.

The $Nd_2Fe_{14}B$ crystal structure is restored after annealing.

d ≈ 10-25 nm

No excessive growth of the soft phase crystallites during the ***short time annealing***.

The crystallite sizes of the annealed 6 h MM samples are smaller than those of the annealed 8 h MM samples [1].

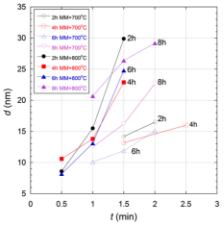

Mean crystallite sizes of α-Fe vs. annealing time for the for the as-milled and annealed samples. The lines are guides for the eye.

The crystallite sizes were determined using the Scherrer formula for the peak with $2\theta = 82.3$ ˚:

$$d = \frac{K\lambda}{\beta \cos\theta}$$

d is the average crystallite size, *K* is the shape factor, *λ* is the wavelength, *β* is the FWHM of the peak and *θ* is the Bragg angle.

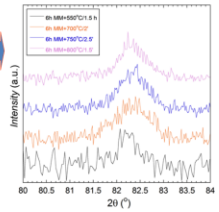

XRD peaks centered at 2θ = 82.3 ˚ corresponding to α-Fe.

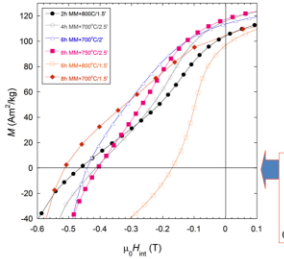

Demagnetization curves for $Nd_2Fe_{14}B$+10% wt. Fe samples 2, 4, 6 and 8 h MM short time annealed: $H_{int}=H_a-M/3$.

The coercivity of the short time annealed 6 h MM samples increases with annealing time.

Progressive restoration of the $Nd_2Fe_{14}B$ crystal structure.

Coercivity decreases with increasing annealing temperature ← larger α-Fe crystallites.

Fe mean crystallite sizes (*d*), coercive field ($\mu_0 H_c$) and remanent magnetization values (M_r) for the $Nd_2Fe_{14}B$+10 wt% Fe 6 h MM annealed samples.

Milling time (h)	Annealing temperature (˚C)	Annealing time (min)	*d* (nm)	$\mu_0 H_c$ (T)	M_r (Am²/kg)
6	700	1.5	10	0.42	114
		2	15	0.44	114
	750	2	20	0.38	124
		2.5	21	0.41	117
	800	1.5	25	0.17	97
	550 [3]	90	34	0.55	115
8 [1]	700	1.5	16	0.51	103
	800	1.5	26	0.54	96

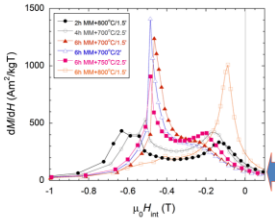

dM/dH vs. *H* curves for $Nd_2Fe_{14}B$+10% wt. Fe samples 2, 4, and 6 h MM short time annealed; $H_{int}=H_a-M/3$.

Low field peaks → badly coupled/uncoupled α-Fe

Higher field peaks → exchange-coupled nanocomposite.

Saturation is not reached up to 10 T.

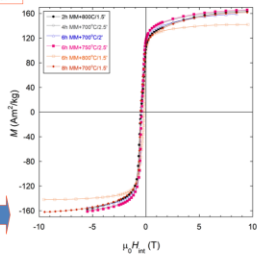

±10T magnetization curves for $Nd_2Fe_{14}B$+10% wt. Fe 2, 4, 6 and 8 h MM samples short time annealed at 700-800 ˚C; $H_{int}=H_a-M/3$.

Progressive decoupling with increasing annealing time/temperature.

Increasingly larger soft phase crystallites and possible phase alterations.

Conclusions:

- ***Short time annealing restores the structure of the hard phase*** destroyed by milling with a ***limited growth of the soft magnetic crystallites***.
- The exchange ***coupling strength*** increases with milling time possibly due to ***smaller soft phase crystallites*** and a better homogeneity of the mixture.
- The ***best exchange coupling*** was obtained for the ***6 h MM*** sample annealed at ***700 ˚C for 2 minutes*** with a maximum coercive field value of ***0.44 T***.
- The ***coercivity*** of the short time annealed 6 h MM samples is ***slightly lower*** than previously reported values on the classically annealed 6 h and short time annealed 8 h MM samples, however, they show a ***higher remanence***.
- The diminishing of the coercivity could be attributed to the pre-milling of the soft phase with benzene.

[1] V. Pop, S. Gutoiu, E. Dorolti, O. Isnard and I. Chicinaş, *J. Alloys Compd.*, **509**, 9964 (2011).
[2] V. Pop, S. Gutoiu, E. Dorolti, C. Leostean, O. Isnard, I. Chicinas and O. Pana, *J. Alloys Compd.*, **581**, 821 (2013).
[3] S. Gutoiu, E. Dorolti, O. Isnard, I. Chicinaş, and V. Pop, *J. Optoelectron. Adv. Mater.*, **12**, 2126 (2010).

Acknowledgment
This work was supported by the Romanian Ministry of Education and Research, Grant No. PN-II-ID-PCE-2012-4-0470.

Conclusions

- **MnBi LTP**: large coercivity at high temperature ⇒ a good candidate for performance spring magnets
- **MnAl:** stabilisation of τ with conservation of Mn moments
- The ***structure and microstructure*** ⇒ strong impact on hard/soft exchange hardness.
- **Intrinsic anisotropy** ⇒ the **strength** of the interphase exchange coupling
- ***Annealing*** linked to the ***recrystallisation temperature*** of soft phases and hard magnetic phases; ***recover*** the crystallinity of the hard phase and ***hinder the increase*** of Fe crystallites.
- For ***higher α-Fe concentration*** the magnetic properties are pourer because non correlation with Fe size crystallites.
- The ***short time annealing*** is more appropriate for higher coercivity of the nanocomposites.

Thank you for your attention

This contribution was supported by the
Romanian Ministry of Education and Research, grant PN-II-ID-PCE-2012-4-0470